British Geological Survey
NATURAL ENVIRONMENT RESEARCH COUNCIL

Reinterpretation of gravity anomalies over the Brabant Massif in southern Flanders (Belgium)

EMGB Programme

Commissioned Report CR/04/215

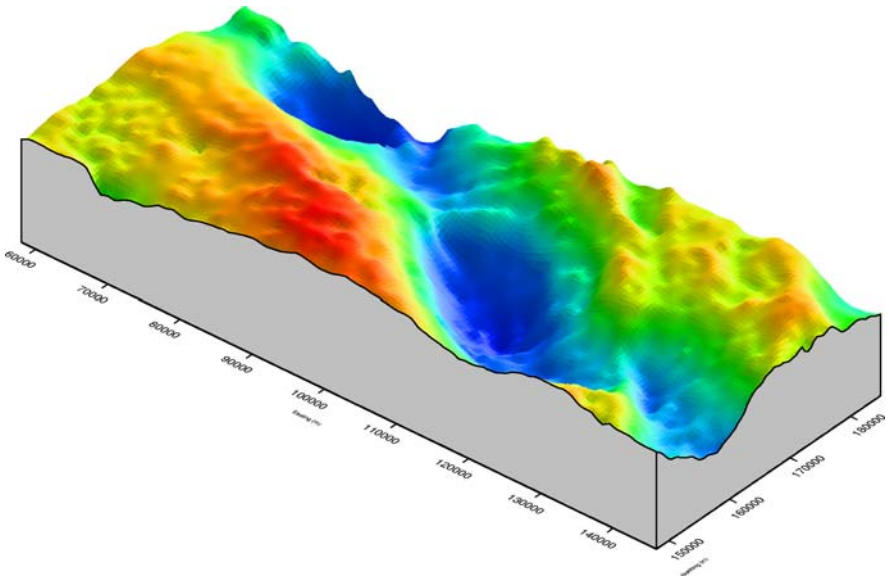

BRITISH GEOLOGICAL SURVEY

EMGB PROGRAMME

COMMISSIONED REPORT CR/04/215

Reinterpretation of gravity anomalies over the Brabant Massif in southern Flanders (Belgium)

B C Chacksfield, J P Williamson, T C Pharaoh and F M McEvoy

Keywords

Gravity; interpretation; geophysics; prospectivity.

Front cover

Perspective view of the residual gravity anomalies after subtraction of the field continued upwards by 5km (viewed from SE).

Bibliographical reference

CHACKSFIELD, B C, WILLIAMSON, J P, PHARAOH, T C AND MCEVOY, F M. 2004. Reinterpretation of gravity anomalies over the Brabant Massif in southern Flanders (Belgium). *British Geological Survey Commissioned Report*, CR/04/215. 47pp.

Keyworth, Nottingham British Geological Survey 2004

Foreword

This report is the published product of a study by the British Geological Survey (BGS) involving reinterpretation of the gravity data over the southern Brabant Massif (Belgium). It complements the report 'Reinterpretation of airborne magnetic data over the southern Brabant Massif in Flanders (Belgium)', which was published in 2003 as BGS report number CR/03/135. The project was managed by GF Consult bvba on behalf of the Ministerie van de Vlaamse Gemeenschap, Afdeling Natuurlijke Rijkdommen en Energie (ANRE).

Acknowledgements

The authors would like to thank Guy Franceschi of GF Consult bvba and Walter De Vos of the Belgische Geologische Dienst (BGD) for their advice throughout this project.

Contents

TABLES

FIGURES

CD-ROM

PDF copy of this report
PDF copy of maps
Project GIS

MAPS (under separate enclosure**)**

Map 1	……	Bouguer gravity anomaly. Scale 1:100 000.
Map 2	……	Residual Bouguer gravity anomaly after subtraction of 5 km upward-continued field. Scale 1:100 000
Map 3	……	Residual Bouguer gravity anomaly after subtraction of 1 km upward-continued field. Scale 1:100 000.
Map 4	……	Horizontal gradient of Bouguer anomaly. Scale 1:100 000
Map 5	……	Verical derivative of Bouguer anomaly. Scale 1:100 000.
Map 6	……	Second vertical derivative of Bouguer anomaly. Scale 1:100 000
Map 7	……	Analytic signal of Bouguer anomaly. Scale 1:100 000.
Map 8	……	Structural interpretation map. Scale 1:100 000.
Map 9	……	Mineral prospectivity map. Scale 1:100 000.
Map 10	……	Structural interpretation map. Scale 1:300 000.
Map 11	……	Residual Bouguer gravity anomaly after subtraction of 5 km upward-continued field. Scale 1:300 000.
Map 12	……	Reduced-to-pole magnetic anomaly with contours of residual Bouguer gravity anomaly (after subtraction of 5 km upward-continued field). Scale 1:300 000.
Map 13	……	Horizontal gradient of Bouguer anomaly. Scale 1:300 000.

Summary

This report describes the interpretation of gravity anomaly data over the Brabant Massif in southern Flanders (Belgium). It is a companion to the interpretation of magnetic anomalies that was undertaken by Williamson et al. (2003).

The interpretation of gravity linears shows a predominant WNW-ESE trend, with a notable absence of significant features with a SW-NE trend. Interpretation of the main negative anomalies over the Brabant Massif, including 2½-D and 3-D modelling studies and calculation of Euler depth solutions, is consistent with the presence of a significant buried granite body with a roof at a depth of 1-2 km, deepening as we move eastwards. Inspection of the maps shows that this body has undergone significant (sinistral?) displacement along major NW-SE structures.

An analysis of mineral prospectivity has been made using the deposit model and a fuzzy logic method of investigation. This study has highlighted the relative importance of the NW and SE corners of the study area, and the importance of intersections between linears of different types.

1 Introduction

This report describes the interpretation of gravity anomalies over the Brabant Massif in southern Flanders. It forms a companion to the reinterpretation of airborne data described by Williamson et al. (2003), which contains much background material that is not repeated here. In addition to interpreting the gravity data for the district, the results were used to enhance the analysis of mineral prospectivity that was first presented in the earlier report. The report is designed to be read in conjunction with the 13 maps at 1:100 000 and 1:300 000 scales that form a separate enclosure.

The limits of the project area for this study coincide with those of the earlier study, which were defined as 58 to 146 km Easting, 148 – 185 km Northing (Belgian Lambert coordinates). The full study, including mineral prospectivity, adheres strictly to these limits for compatibility with the earlier work. An expanded area, defined as 20 – 260 km Easting, 138 – 245 km Northing, was used in image production, identification of linear features and map production at 1:300 000 scale, but a rigorous interpretation over the entirety of this wider area was not attempted. The project area is illustrated in Figure 1.

2 Data processing and transformations

2.1 DATA PROCESSING

Data were initially supplied to BGS in the form of Surfer grids at 1 km node spacing, using reduction densities of 2100 and 2670 kg.m^{-3}. Preliminary imaging showed that this data spacing was too coarse to resolve short-wavelength anomalies within the study area, so more closely distributed scattered data were requested and subsequently supplied in an Excel spreadsheet, also at reduction densities of 2100 and 2670 kg.m^{-3} (De Vos, pers. comm.). All further processing was carried out using the 2100 kg.m^{-3} data, as this was deemed the more appropriate density to minimize the effect of topography in the majority of the district.

Data processing operations were carried out using version 5.1.8 of Geosoft Oasis Montaj, which provides interactive facilities for manipulating and displaying the data. Both the scattered and gridded data sets were converted into comma-separated value files and merged into one dataset before being imported into Geosoft as a single database.

The resulting Geosoft database channels (which are equivalent to the Excel spreadsheet fields) were given the same names as the original datasets. A data mask was created around the edge of the scattered data so as to exclude the gridded data within the area covered by the scattered data; the subsequent masked data were output to new data channels.

The merged data set was then gridded in Geosoft using a minimum-tension algorithm, with grid node spacing set at 500 m and the blanking distance set at 5000 m. The resulting grid was inspected for errors, and it became apparent that the scattered data were noisy in some areas where individual surveys overlapped and also at the boundary between different surveys. Scattered data exhibiting these problems were masked out in preference for the grid node data, which were smoother, possibly because these problems had already been rectified during the processing of the data. Further masking was carried out to provide a mostly seamless join between the scattered and gridded data. These problems could largely have been avoided if a processed data set had been made available in the first instance.

Subsequent re-gridding revealed a few isolated data errors within the onshore scattered data, and eight errors were manually deleted and output to an errors data file. Local errors within the grid node dataset were retained, as these were outside of the main study area. Offshore, a northeast trending stripy pattern was found to be spatially coincident with ship-track locations and was deemed to be artificial; these data were retained but were masked out on the images and maps.

The final 'clean' dataset was output as an ASCII file and was later used to generate a variable density grid based upon the gravity station elevations (see section 2.4).

2.2 GRID CONVERSION AND TRANSFORMATIONS

The grid resulting from the processing described in section 2.1 was converted from the Geosoft grid format (`*.grd`) to a BGS in-house standard grid format (`*.sg`). It covers the area Easting 20000 m to 260000 m and Northing 138000 m to 245000 m (Lambert coordinates).

Software developed within BGS was then used to perform transformations of the gridded data, including calculation of vertical and horizontal derivatives and upward continuation. Computation of the analytic signal was calculated using an algorithm within Geosoft. Williamson et al. (2003) give a detailed description of these transformations and their uses in their Appendix 2.

Before use in the ArcView geographic information system (GIS), the gravity grids were interpolated to a 250 m cell size; this was done in order to reduce the pixel size so that the resulting grid images were appropriate for viewing at 1:100000 scale. The grids were then converted into ArcView ASCII raster format, ensuring that grid nodes were geo-registered centrally relative to ArcView image pixels.

In addition to the gravity grids, a reduced-to-pole magnetic grid resulting from the 2003 study was windowed to Easting 20000 m to 260000 m and Northing 120000 m to 245000 m in order to allow data extraction along profiles for 2½-D modelling, and also for display of the magnetic and gravity data together in image form.

In order to compare the potential field data with topography, a 100 m DEM was produced using data from the Shuttle Radar Topography Mission (SRTM). This dataset covers the majority of the land masses of the Earth at a native resolution of 90 m, and is freely downloadable from the internet. The vertical accuracy of the uncorrected data is relatively poor (the target absolute vertical accuracy is 16 m), but the data are precise, and show a wealth of topographic detail. This dataset has been incorporated into the project GIS, as well as forming the backdrop to Figure 1.

2.3 PRODUCTION OF GEOPHYSICAL IMAGES

Geo-registered colour shaded relief images were generated in version 5.1.8 of Geosoft Oasis Montaj as high resolution JPEG images with a pixel size of 50 metres, and are therefore suitable for display and printing at 1:100000 scale. The images cover the area Easting 20000 m to 260000 m and Northing 120000 m to 245000 m. Additionally, a colour scale was generated for each image and stored as a separate file in TIFF format. The final maps were created from customised ArcView layouts at two map scales: the regional maps of the northern Brabant Massif were mapped at 1:300 000 scale, and the detailed study area were mapped at 1:100 000 scale between coordinates 58000m to 146000m East and 148000m to 185000m North (the same area as for the earlier magnetic study). A mask was applied to all the regional gravity images to remove the data offshore.

2.4 VARIABLE-DENSITY GRAVITY REDUCTION

Uniform application across the entire district of a Bouguer reduction density of either 2670 $kg.m^{-3}$ (appropriate in the southeast) or 2100 $kg.m^{-3}$ (appropriate everywhere except the

southeast) introduces artefacts that are due to an incorrect density assumption for the rocks that lie between sea level and the topographic surface. By processing the data with a Bouguer reduction density that varies according to the nature of this material, first-order topographic effects can be suppressed, thereby allowing a clearer view of anomalies arising from the underlying geology. This improvement can be especially pronounced in shaded relief images of the data.

The problem of computing the variable density Bouguer reduction is principally an issue of how best to derive a representative reduction density at each gravity station. The approach taken here is to estimate the proportion of basement rocks in the column of material between the observation point and sea level. We also note that there is a linear relationship between reduction density and Bouguer anomaly, which means that given values of the Bouguer anomaly at a fixed point using two reduction densities (as supplied), it is possible to compute the anomaly value at any other density (it is probably better to use the terrain correction at each station to effect this recalculation, but this information was not available).

A data file containing the depths of intersection of Palaeozoic basement within boreholes in the Brabant Massif was supplied (De Vos, pers. comm.). These data were used to generate a grid of the depth to basement of the Brabant Massif within the district, which can then be interpolated at any point to give an approximate value of the depth to Lower Palaeozoic rocks. The density at each station is then estimated from the proportion of basement material above sea level. As an equation we may write:

$$\rho = \rho_{cover}.(z_{topo} - z_{bsmnt}) + \rho_{bsmnt}.z_{bsmnt}$$

where ρ_{cover} and ρ_{bsmnt} are the densities of 'cover' and 'basement' respectively, z_{topo} is the topographic elevation at that point, z_{bsmnt} is the basement depth. Note that this estimate only needs to be done where $z_{bsmnt} > 0$, because elsewhere it is appropriate to use a reduction density equivalent to the cover density. The reduction density thus varies between ρ_{cover} and ρ_{bsmnt}. The results of applying this processing to the scattered data are shown in Figure 2.

3 Regional interpretation of gravity data

Maps 8 and 10 are structural summary maps showing the main features derived from the geophysical images. This section of the report references linears and other features that are named on these maps. Gravity linears have been classified into 9 categories, of which the majority are maxima (peaks) and minima (troughs) picked from the observed, residual and derivative gravity maps. Solid lines represent longer persistent linears, and dashed lines indicate local discontinuous features. Inflections (gradients) were primarily picked from the horizontal gradient map. Gravity highs and lows derived from the 5 km residual gravity field are shown as coloured polygons, where pale colours represent broad regional features and darker colours indicate local higher amplitude anomalies lying within the regional features. 3D Euler deconvolution depth solutions are shown as coloured dots classified at 1000 metre depth intervals.

Within the project area, three structural domains are recognised on the basis of the gravity images:

1. Southwestern domain (Domain 1)

This domain corresponds with the area SW of a line from Kortrijk to Soignies and is characterised by a regional positive gravity anomaly and strong residual gravity high over its northeastern part, with numerous associated linears. The residual anomaly becomes more subdued towards the SW, and NW towards the Channel coast.

2. North and central domain (Domain 2)

This domain lies to the NE of Domain 1 and is dominated by a belt of strong negative gravity anomalies, within which three major residual gravity lows can be identified. GL1 in the NW [min value -12 mGal], centred on Oostrozebeke, the more extensive GL2 [min value –12 mGal] in the centre, whose minimum is located SE of Brakel, and GL3 in the east [min value –4 mGal], centred on Halle. Fewer linears are recognised in this domain.

3. Northeastern domain (Domain 3)

This domain refers to the area NE of Domain 2, beyond a line from Petegem to Zandbergen (not shown), and extends outside of the study area to the north and east into the expanded area. It corresponds to an intermediate level of gravity anomaly amplitude, with a moderate number of recognised lineaments. Three distinct NW-trending gravity highs occur within this domain.

3.1 RELATIONSHIP OF GRAVITY LINEARS TO GRAVITY HIGHS AND LOWS

Domain 1 is characterised by several WNW-trending linear maxima e.g. L1, and linear inflections, e.g. L2, with some deviation to a more W-E trend in the south, e.g. L14. These are associated with the crest of the residual positive gravity anomaly which dominates this domain and are up to 25 km in length. A number of shorter linear inflections e.g. L3, have a SW-trend.

Domain 2, in contrast, has fewer continuous linears, but many shorter linears with a variety of types and trends.

In the belt of transition between Domains 1 and 2 the linears are mainly short, sub-parallel, of inflection type and generally of a NW-trend, parallel to the margins of the main gravity lows (e.g. L4). A few longer linears of minimum type, and short linears of maximum type, have a comparable trend (e.g. L5). A further series of NW-trending inflections run along the northern margin of the belt of gravity lows between Domains 2 and 3.

Within Domain 2 itself a few NW trending continuous linears occur within or along the margins of gravity lows GL1 and GL2. One of these, a NW trending maximum, marks a gravity ridge that divides GL 1 into two separate local gravity lows. Other linears are shorter and more arcuate, for example at the SE end of GL2 (SE of Geraardsbergen), where a series of arcuate short linears swing into a more northeasterly orientation (e.g. L6), and appear to be associated with the southern margin of GL 2. Other linears of a similar nature are associated with the southern margin of GL 1.

Between gravity lows GL1 and GL2, and in the transition from Domain 2 to Domain 3, are a number of types of linear arranged concentrically around the gravity lows e.g. L7. A similar relationship is observed around GL3, e.g. L8, L9.

Domain 3 contains a number of long (up to 20 km) NW-trending linear maxima (e.g. L10, L11, L12 and L13). L11 is particularly notable, as it is long (30 km) and extends beyond Domain 3, crossing Domain 2 (where it appears to offset GL3 from GL2), approaching Domain 1. Linear L12 is comparable, as it extends from Domain 3, crossing into Domain 1 to the SE of the project area. Note that linears L11 and L12 lie on both sides of the gravity low centred at Halle (GL3). Several other shorter linears of inflection and minimum type lie parallel to these major linears.

3.2 RELATIONSHIP OF GRAVITY LINEARS TO MAGNETIC LINEARS AND ANOMALIES

The relationship of the gravity linears to the magnetic linears described in the previous report (Williamson et al., 2003) will now be described. Linears L1 and L2 do not correspond to magnetic linears of significant length. Some SW-trending magnetic linears may correspond to L3 however. The same is true of L4 and L5, which have comparable size and orientation to magnetic linears in the vicinity of MH5. L6, 7 and 8 show poor correspondence with magnetic linears. L9 corresponds well with W-trending linears of offset type, e.g. Offset 3 (Lennik-

Anderlecht) and Offset 7 (St-Pieters-Leeuw) which are inferred to displace the prominent magnetic linears internal to MH1 (Williamson et al., 2003). L10 and L11 correspond well to the strong magnetic gradient (and linear) at the western edge of the prominent magnetic high (Aalst-Halle Magnetic High, MH1) associated with the Tubize Group. The trend of L10 and L11 is parallel to that of the numerous internal magnetic crest and trough anomalies within MH1. Note however that while the magnetic anomalies maintain their character along the length of this zone (except for the zone of structural disturbance noted in the Halle district), the character of L11 changes markedly along its length. L12 and L13 are comparable in location and orientation to the magnetic linears at the eastern flank of MH1.

3.3 INTERPRETATION OF GRAVITY LINEARS

L1 coincides with the faulted boundary of the Devonian-Carboniferous filled Namur Basin as shown on the map of De Vos et al (1993). Linears L2, L4 and L5, dominantly of inflection type, may be associated with discontinuous segments of the Nieuwpoort-Asquempont Fault Zone (De Vos et al., 1993; Mansy et al., 1993). Gravity linears lying between these two major fault zones, may reflect a dominant WNW-ESE structural grain within the gently deformed Early Palaeozoic sedimentary rocks in this region. Gravity linears L6, L7 and L8, mostly inflections, and concentrically arranged around the prominent gravity lows GL2 and GL3, are presumed to be related to the origin of the latter. Their SW- and W-trending orientation is at variance to the known NW-trend of fold structures and cleavage throughout the project area. These observations are compatible with an origin during emplacement of hypothetical discrete igneous intrusions within Domain 2, but not (apparently) with the Acadian penetrative deformation presumed to have produced the strong magnetic fabric in at least part of the Anglo-Brabant Deformation Belt. L11 and L10, its extension to NW, are likely associated with the Asquempont Lineament, as defined by Sintubin et al. and Sintubin & Everaerts (2002). They, together with L12 and L13, parallel the internal magnetic structure of MH1, and are likely associated with the structural evolution of that block, principally involving the deposition and deformation of the Tubize Group metasedimentary rocks. Besides their length and continuity, another notable feature of L11 and L12 is that they both compartmentalise the regional gravity low of Domain 2, and apparently offset (with a sinistral sense) the feature(s) which cause it. Other linears (e.g. L9) may correlate with inferred shear zones which apparently displace the dominant magnetic grain within MH1, and may relate to a later, possibly Variscan phase of deformation (Williamson et al., 2003).

3.4 COMPARISON WITH PREVIOUS STRUCTURAL INTERPRETATIONS

Published structural models for the project area e.g. De Vos et al. (1993), Van Grootel et al. (1997) and Mansy et al. (1999) have emphasised the increasing magnitude of strain and metamorphic grade from SW to NE, compatible with the transition from shelf to deep water basin, and from platform to deformation belt, along the northern margin of Avalonia, comparable to the situation in eastern England (Pharaoh et al., 1987; Pharaoh, 1999). A further aspect of this model is the proposed presence of granitoid plutons to explain the prominent gravity lows characteristic of Domain 2. These postulated granites are considered to have buttressed the southern part of the area, shielding it from intense Acadian deformation (Mansy et al., 1999). By contrast, the compressional wedge model proposed by Sintubin (1999) and Sintubin & Everaerts (2002) implies greater symmetry of deformation, with a rift filled by Cambrian Tubize Group inverted during Acadian deformation into a compressional wedge, overthrusting foreland basins to north and south. The proposed boundaries of the compressional wedge lie at the Asquempont and Tienen Lineaments. In this model, the role of the postulated granites during deformation is less significant, and indeed, Sintubin & Everaerts (2002) argue that the pattern of gravity lows in Domain 2 is a consequence of the interaction of rigid blocks of Precambrian basement (albeit of possibly granitic composition).

The observations and interpretations described above do not allow one or other of these models to be validated. The gravity linears confirm the dominantly NW-SE trending orogenic grain already known from geological and aeromagnetic observations, but the exact cause of the linears is unknown. Many correspond to well-known structures e.g. the edge of the Namur Basin (L1), the Asquempont-Niewpoort Fault Zone (L2, L4) and the Asquempont Lineament (L11). The apparently polygonal-concentric pattern of gravity linears around the gravity lows of Domain 2 (e.g. L5, L7, L8) could have been generated by forceful intrusion of the postulated granite plutons. Gravity linears L11 and L12 are associated with apparent dextral offsets (and compartmentalisation) of the regional gravity low, supporting the interpretation of Sintubin (1997) of dextral transpression along NW-SE trending zones such as the Asquempont Lineament. However, the relative age of the geological structures causing the linears, and the features causing the gravity low, is unclear. If the gravity low is indeed due to granites for example, two emplacement models are possible: firstly a number of relatively small plutons could have been emplaced into an existing belt of transtension (with discrete dilatant voids) in the crust; alternatively, one very large batholith could have been disrupted by shear zones post-emplacement. The first of these models is the more plausible mechanism of magmatic emplacement.

4 Depth solutions

A description of the theoretical background to source depth estimation from potential field data is given in Williamson et al. (2003) (their Appendix 4). In contrast to aeromagnetic data, gravity data are generally not collected as profiles and it is therefore more natural to study source depths using 3-D deconvolution techniques based on a grid of the data. In this case, Euler and slope depth solutions were computed from the 0.5 km grid of Bouguer anomaly data (reduction density 2100 $kg.m^{-3}$) using in-house software. For the Euler solutions a structural index of 1 (line mass) was deemed most appropriate for representing steep contacts.

When computing 3-D depth estimates, an externally calculated grid of the vertical derivative must be supplied. As noted in Williamson et al. (2003) Appendix 4, the vertical derivative transform tends to amplify very short-wavelength features in the data, which can lead to a preponderance of shallow solutions. By applying some smoothing to the data prior to computation of the vertical derivative it is possible to suppress the very short wavelength features and improve the quality of the depth solutions computed. By a process of trial and error, upward continuation of the data by 0.5 km was found to strike an acceptable balance between smoothing the data and preservation of gradients. The computed Euler depth solutions are shown in Figure 3, and are also superimposed on Maps 8 and 10.

5 2½-D modelling

The results of 2½-D geophysical modelling along four transects across the area, shown to a maximum depth of 15km were published by Everaerts et al. (1996). The models showed that the gravity lows could be modelled as a granite intrusion with a top surface at a depth ranging from approximately 1 km to 4 km, with magnetic rocks of the Tubize Group, lying over the granite batholith at depth, being responsible for the observed aeromagnetic anomalies.

For the 2003 magnetic interpretation project, a single 2½-D model was constructed along a transect through the area between points [138000 148000] and [138000 185000], using data extracted from grids. This simple model again showed that the observed anomalies in the region could be explained by a granitic intrusion at approximately 3 km depth, overlain by magnetic rocks of the Tubize Group, in turn flanked by the non-magnetic Blanmont Formation.

For the current study two profile models were constructed across the eastern part of the Brabant Massif primarily across the easternmost gravity low to test whether this anomaly was caused by the same granite body as that identified from the previous modelling, thought to be buried at a deeper structural level.

Profile 1 is aligned north-south from [180000 138000] to [180000 245000], and profile 2 is a NE-SW profile from [175000 138000] to [215000 245000] which intersects profile 1 within the gravity low (Figure 4). Both profiles are oriented obliquely to the inferred strike, but are more perpendicular to the main gravity anomaly trend. The locations of the tops of each geological polygon were interpreted from the geological sub crop map by DeVos et al., and each polygon represents a stratigraphical unit based upon this map.

Model 1 (Figure 5) shows that the main gravity low and accompanying series of magnetic highs can be modelled as a steep sided low density granite body at a minimum depth of 2 km overlain and surrounded by magnetic Tubize group sediments. The shape of the intrusion is comparable in depth and width to the granite(s) further to the west, providing strong evidence for a continuous granite batholith extending across most of the northern Brabant Massif. The Tubize Group is shown as a generally moderately magnetic unit (0.005 SI units) containing a strongly magnetic layer (0.025 SI units). The observed magnetic anomalies are assumed to be caused by irregularities in the top and bottom surfaces of this layer due to folding and faulting. In contrast with the 2003 modelling, it was found not to be necessary to increase the susceptibility of the Tubize Group overlying the granite plutons. Possible explanations for this are an absence of contact metamorphism in the rocks adjacent to the intrusion or a uniform magnetite content due to primary compositional homogeneity. Structural complexities such as small scale overturned folds and thrust displacements, compatible with structures observed in the Tubize Group at outcrop, were introduced into the magnetic unit to improve the fit of the model, although these are necessarily somewhat schematic.

The structure surrounding the granite is that of an antiform, with the magnetic high at 35km along the profile modelled as a major secondary fold developed on its northern limb. This structure would explain the magnetic high to the north of and parallel to the mapped extent of the Tubize Group over much the region. To the south of the granite, the sharp change in the magnetic anomaly pattern suggests that the strongly magnetic Tubize unit is abruptly terminated by a major fault.

Gravity highs on either side of the gravity low are attributed to higher density (2.75 $Mg.m^{-3}$) Tremadoc, Middle and Upper Ordovician, and Silurian rocks (grouped together as a single polygon on the model). The steep gradients characterising the margins of the gravity low are generated by the abrupt density contrast between these rocks and the lower density Middle to Upper Cambrian formations and Tubize Group (2.70 – 2.72 $Mg.m^{-3}$) as well as by the granite body.

In the northern part of the model a gradual decrease in gravity accompanied by a relatively smooth magnetic profile signifies non-magnetic lower density Upper Palaeozoic and younger rocks becoming progressively thicker within the Campine sedimentary basin.

Profile 2 (Figure 6) shows a good agreement with profile 1 and confirms the presence of a granite body beneath magnetic Tubize Group rocks. The magnetic high at 35 km along the profile has the same amplitude and shape as that of profile 1, helping to confirm the interpretation of a major secondary fold at depth.

However, the magnetic anomaly profile over the granite is less subdued than on profile 1, implying that the top of the strongly magnetic Tubize Group unit has to be at a shallower depth and that the rocks may be more tightly folded to account for this. It is also necessary to increase the magnetic susceptibility to 0.04 SI units to match the anomaly amplitude and still maintain a comparable thickness of magnetic Tubize Group. A direct comparison between the southern ends of the profiles is complicated by faulting, and the two profiles are not parallel, but the change in

depth to the top of the Tubize Group is consistent with the geological map and it would appear to confirm the existence of a major fault with a down throw to the east.

The steep decrease in gravity to the north reflects the presence of a thickening of lower density rocks within the Carboniferous and younger sediments of the Campine Basin flanking the NE margin of the Brabant Massif.

6 3-D modelling

The 3D modelling area was defined as 35 to 225 km Easting, 138 to 208 km Northing, an area that includes the main anomalies that are assumed to be sourced within basement rocks. These coordinates were used to define the limits of data extraction from the cleaned grid of Bouguer anomaly data reduced at 2100 kg.m^{-3}. The regional field was modelled by fitting a plane to these data by least squares, where the form of the regional field $R(x, y)$ is assumed to be:

$$R(x, y) = ax + by + c$$

where a, b and c are coefficients that define a planar regional. In this case, a=7.10503, b=-0.522044 and c=0.655492.

After removal of the regional field, the residual field was continued onto a level surface above all topography (at 240 m above sea level) using an equivalent source technique (Blakely, 1997). This 'drape-to-level' continuation is essential when using frequency domain techniques to model onshore gravity data (usually collected on an irregular topographic surface), as it safeguards against certain errors that can arise in the process of continuation onto an uneven surface. Although drape-to-level continuation is not necessary for modelling in the space-domain, by undertaking this data processing step we can integrate both modelling techniques into the overall computational scheme.

Using available borehole information (De Vos, pers. comm.) and contours of the depth to basement (Verniers et al., 2001) a grid of the top basement was constructed (here taken as the top of the early Palaeozoic). This simple model of the top basement surface does not include faults, and in overall form is seen to slope downwards to the northeast, with depths below sea level ranging from –0.18 km (exposed early Palaeozoic rocks in the southeast of the district) to 0.70 km in the northeast corner of the district. Density information on the cover sequence rocks is scarce, and an assumed model was used in which density increases from 2100 kg.m^{-3} at and above sea level to 2400 kg.m^{-3} at a depth of 1 km. The rationale behind choosing this model of cover density is that the lowest value is most appropriate at surface, as can be seen in the selection of Bouguer reduction density, but is unlikely to persist at depth due to the effects of compaction and saturation. The maximum density that was used is an assumed value based on measured densities in other settings. While it is recognised that there is considerable uncertainty in the choice of density model, significant thicknesses of cover sequence rocks occurring towards the NE of the district should have only limited influence on the 3D model of the granite batholith. The gravity effect of the cover sequence model was then computed on a level computation surface at a height of 240 m using a frequency-domain method, assuming a basement density of 2700 kg.m^{-3}. The resulting anomaly was subtracted from the levelled residual to give the gravity anomaly field stripped to the top of the early Palaeozoic.

The stripped field contains high frequency anomalies that increase in magnitude eastwards. Conceptually, these anomalies are thought to have their sources within Palaeozoic rocks that progressively overstep the postulated granite towards the east. In order to avoid building these anomalies into the 3D model of the granite it is necessary to apply a wavelength filter to discriminate between high frequency anomalies assumed to be sourced within the early Palaeozoic sequence and longer wavelength anomalies that are due to the postulated granite. Frequency-domain filtering was performed using the GMT program 'grdfft', using wavelengths

of 10 km and 6 km for the high-pass and high-cut parameters respectively (these parameters were found by a process of trial and error). The final residual field used as input to the 3D modelling process is shown in Figure 7.

3-D modelling of the negative residual anomaly was undertaken with the in-house program GM3D, which uses a space-domain, prism-based method to adjust automatically the top and/or the base of the desired unit (Rollin, 1988). In this case, the modelling scheme was chosen so that the top and base of a low-density layer with starting thickness zero were adjusted on alternate iterations, with the residual anomaly at each step being partitioned in the ratio 1:1 between the top and base surfaces. The starting depth for the top and base surfaces is an arbitrary parameter, and was here set to 6 km below sea level. After 10 iterations, the minimum calculated value has approached the minimum residual value to <1 mGal.

The results of modelling are shown in Figures 8 and 9. Figure 8a displays the top of the granite surface; Figure 8b shows the total granite thickness. Figure 9 displays cross-sections through the model along lines coincident with the four profiles published by Everaerts (1996).

7 Re-evaluation of the mineral potential of the southern Brabant Massif

7.1 INTRODUCTION

This work is a re-evaluation of the mineral potential of the Lower Palaeozoic rocks of the Brabant Massif in the light of re-interpreted high-resolution gravity data and a review of recently published literature. It builds on a pilot mineral prospectivity appraisal, using the 1994 aeromagnetic data, that was undertaken by the British Geological Survey (Williamson et al., 2003).

In the Lower Palaeozoic of the Brabant Massif, several occurrences of polysulphide mineralisation have been identified, especially (but not exclusively) along the southern margin of the Anglo-Brabant deformation belt. By studying polished sections, Dandois (1997) found traces of polysulphide mineralization, showing discrete mimerals of at least two of the metals Cu, Pb and Zn in 20 different locations, mostly in vein systems, but also in tectonic breccia and as disseminations in magmatic rocks.

In 1988, and later from 1996 to 2000, drilling at Sint-Pieters-Kapelle in the Marcq area intersected polysulphide mineralisation in a low-angle reverse shear zone. Further mineralisation was subsequently discovered at Bierghes, in the Senne valley, within the same high strain zone. This mineralisation has been interpreted as mesozonal orogenic vein mineralisation formed during the tectonometamorphic deformation of the Anglo-Brabant Massif (Piessens et al., 2002).

Mesozonal orogenic vein deposits, commonly referred to as greenstone-hosted, turbidite-hosted or mesothermal (Groves et al., 1998), are important gold producers worldwide, typical examples of which are the Archaean lode gold deposits, and similar deposits within the Palaeozoic, Mesozoic and Cenozoic. These accumulations often occur with polysulphide mineralisation that is associated with the gold bearing fluids.

This desk-based mineral prospectivity analysis for the potential of mesozonal orogenic vein mineralisation in the Brabant Massif was conducted within a Geographic Information System (GIS) environment using Arc Spatial Data Modeller (SDM) software (Kemp et al., 2001). The assessment builds upon the prospectivity analysis carried out in 2003 by implementing the following key revisions: (i) the incorporation of re-interpreted high resolution gravity datasets, both the horizontal gradient and the derived gravity lineaments; (ii) the omission of the De Vos

et al. (1993) fault dataset; (iii) the re-evaluation of the role of magmatic fluids in the evolution of these deposits.

7.2 MINERAL PROSPECTIVITY ANALYSIS

Mineral deposit models are syntheses of large amounts of data that provide an essentially qualitative basis for exploration and resource assessment. Such models can be used to identify the key exploration criteria for a particular type of deposit and thus form the basis for analysis of the mineral potential of a region. The standard platform in mineral exploration to coordinate and manage these datasets has become the GIS, which facilitates querying and analysing the data in order to determine those parameters which are critical or subsidiary to the mineralisation process. GIS technology also allows the structured integration and modelling of these often-voluminous datasets that is necessary to look for patterns and associations that may otherwise not be apparent.

All methods of prospectivity analysis combine two or more evidential themes to generate a response theme that is a map predicting favourable locations for mineral deposit occurrences. Detailed background material, including the theory behind the software used to perform the mineral potential mapping is given in Williamson et al. (2003). In this case, Fuzzy Logic was selected as the most appropriate method for the analysis of mineral prospectivity in the Brabant Massif study area, as it is a knowledge-based method that does not require 'training' from known mineral occurrences, and is thus suitable for study areas in which there are few known occurrences.

In the Fuzzy Logic method, the expertise of the explorationist is used to determine the relative significance of each type of exploration data and then to search for patterns which reflect the total effect of such significance. In practice, this means selection of appropriate data layers for the analysis and the assignment of a relative weight in the range zero to one to each layer in order to indicate its significance. The total effect is then computed using established rules for combination of fuzzy quantities (Williamson et al., 2003). Fuzzy Logic prospectivity analysis has been applied with success over a number of different deposit types worldwide including Mississippi Valley Type (MVT) mineralisation (D'Ercole et al., 2000), porphyry copper deposits in northern Iran (Tangestani and Moore, 2003), and mesozonal orogenic gold deposits in the Yilgarn Block, Western Australia (Groves et al., 2000).

Prospectivity modelling in the Lower Palaeozoic rocks of the Brabant Massif was based on a series of procedures summarised below:

1 Selection of target mineralisation within the Brabant Massif (mesozonal orogenic mineralization);

2 Review of the deposit model for mesozonal orogenic mineralisation to determine key exploration indicators;

3 Assessment of the capability of available data to provide the key indicators;

4 Data processing, interpretation and analysis to extract key indicators

5 Assignment of weightings, zones and styles of influence to key indicators (expert parameterisation);

6 Calculation of prospectivity using Fuzzy Logic model

7.3 FUZZY LOGIC MODEL FOR MESOZONAL OROGENIC MINERALISATION IN THE BRABANT MASSIF, BELGIUM

Of the twenty or more occurrences of vein style mineralisation that have been identified from boreholes in the Brabant Massif region, the only two localities that have been documented in any

detail in internationally available publications are Sint-Pieters-Kapelle in the Marcq area (Piessens et al. 2002, Piessens et al. 2000, Piessens et al. 1999) and the Bierghes Sill (Dewaele & Muchez 2004, Dewaele et al. 2003). The mineralisation in both areas shares many key characteristics with that of mesozonal orogenic mineralisation, the key features of which are discussed below.

7.3.1 Mesozonal orogenic vein deposits

Orogenic gold deposits, commonly referred to as greenstone mesothermal gold, are well documented. These deposits have been summarised in a variety of comprehensive ore-deposit model descriptions that include Hodgson (1993), Groves (1998) and Nesbitt (1991). A brief description of these deposits after Robert *at al.* (1997) and Groves et al. (1998) is provided below.

Orogenic gold deposits are formed during compressional to transpressional processes at convergent plate margins in accretionary and collisional orogens. These deposits typically consist of quartz-carbonate veins in moderate to steeply dipping brittle-ductile shear zones and locally in related shallow-dipping extensional fractures. They are commonly distributed along major fault zones. Veins have strike- and dip-lengths of 100 m to 1000 m, either singly or, more typically, in complex vein networks. They are hosted by a wide variety of lithologies, but there are district-specific lithological associations. The veins are dominated by quartz and carbonate, with lesser amounts of chlorite, scheelite, tourmaline and native gold; pyrite, chalcopyrite and pyrrhotite comprise less than 10 % of the veins by volume. The ores are gold-rich and have elevated concentrations of As, W, B and Mo, with very low base metal concentrations. Despite their significant vertical extent (commonly > 1km), the deposits lack any clear vertical mineral zoning. Wallrock alteration haloes are zoned and consist of carbonatisation, sericitisation and pyritisation. Halo dimensions vary with the composition of the host lithologies and may envelope entire deposits in mafic and ultramafic rocks.

The mineralisation in both the Marcq area and the Bierghes area share many characteristics with published examples of orogenic vein deposits. Table 1 summarises the typical features of orogenic mesozonal deposits and compares and contrasts it to the mineralisation at Sint-Pieters-Kapelle and in the Bierghes Sill.

	Typical	**Marcq Area (St Pieters Kapelle)**	**Bierges Sill**
Tectonics	In accreted, deformed and metamorphosed continental margin or island arc terrains. Close to major structures; faults or major shear zones	Cambrian core bordered by Ordovician-Silurian foreland basin. A late Ordovician magmatic arc has been postulated between them. High strain zone comprising both low angle reverse and high angle shear zones.	
Size and grade	Up to a few million tonnes, typically 5 - 25 ppm	Sub-economic	
Host lithology	Widely variable; greywackes-pelites, chemical sediments, volcanics, ultramafics. Local control by competence contrasts in host succession	Mineralisation occurs in quartz veins within turbiditic sequences (alternation of siltstones and pelites). Few interstratified magmatic rocks.	Mineralised quartz-carbonate veins intruded into a dacite metaporphyry sill.
Metamorphism	Variable; commonly greenschist	Regional greenschist (weakly metamorphosed)	
Relations to plutons	Variable	A granitoid body is inferred at depth from gravimetric data. Magmatic rocks occur in the vicinity, although ~30Ma older. A magmatic origin of fluids is unlikely from structural and time relationships and geochemical characteristics.	

	Typical	Marcq Area (St Pieters Kapelle)	Bierges Sill
Regional geochemistry	Prospective belts regionally enriched in As, and locally Sb, relative to average crustal abundances	Regional geochemical signature masked by veneer of Mesozoic and Tertiary cover rocks.	
Local structure	Ores in dilatant zones controlled by folds and faults; mineralisation commonly associated with second-order faults related to major structures. Shear zone/fault intersections and bends particularly favoured	Low-angle reverse shear zone postulated to converge at depth with a major, NW-SE high-angle tectonic dextral transpressional shear zone (Asquempont FZ)	Veins occur in the Oudenaarde-Bierghes FZ, part of the Asquempont FZ. Strong tectonic control along NE dipping zones parallel to fracture/cleavage planes.
Timing	Late; post-dates main deformation	Shear zones formed in Early Devonian Acadian Orogeny (around 400 Ma). Veins are syn-tectonic 373+/-11 Ma and cut cleavage, thus post-dating main deformation event. Mineralisation, alteration and deformation occurred during the late stages of the Acadian Orogeny (373+/-11)	
Ore morphology and textures	Quartz veins, typically banded, occasionally vuggy with high-grade ore shoots; vertically continuous	Mineralisation occurs in small deformed quartz veins and disseminated in host rock	Mineralisation occurs in several small lenses, up to one metre thick. Total thickness of mineralised zone is 50m
Mineralogy and paragenesis	Early phases with quartz, Ca-Mg-Fe carbonates, arsenopyrite, pyrite, albite, sericite, chlorite, scheelite, stibnite, pyrrhotite, tetrahedrite, chalcopyrite, tourmaline. Late phases with gold, galena, sphalerite, tellurides	First phases with quartz, pyrite (stage 2), arsenopyrite, marcasite (stage 3a), sphalerite, chalcopyrite, galena, stibnite and minor pyrrhotite, muscovite, chlorite, iron-rich calcite, siderite (stage 3b), pyrrhotite (stage 3c).	Sulphides are restricted to first phase vein generation. First phase: dolomite, pyrite, chalcopyrite, galena and quartz. Second stage: dolomite and quartz. Third stage: quartz
Hydrothermal alteration	Carbonatisation, albitisation, sericitisation, silicification, sulphidation, chloritisation.	Regional chloritisation. Local envelope of intense silicification and sericitisation	Pattern of carbonatisation, sericitisation, silicification and chloritisation
Litho-geochemistry	Au/Ag typically > 1; associated Ag, Sb, As, W, Hg, Bi, Mo, Pb, Zn, Cu, Ba.	Pb, Zn, Cu, As. Limited information available.	
Fluid inclusions and isotopes	Low salinity, T = 250 - 350 C. Crustal sources.	Low salinity, T = 250 – 320 (minimum). Metamorphic fluids (crustal)	Vein generation (VG) 1:T = 341-363 C. VG 2: T = 235 and 265 C. Metamorphic fluids (VG 1 & 2)

Table 1 Simplified deposit model for mesothermal lode gold and associated polysulphide mineralisation

The mineral deposit model underpinning the prospectivity modelling carried out in 2003 was that of turbidite-hosted orogenic mesothermal gold deposits, and was selected primarily on the features of the mineralisation in the Marcq area. However, subsequently published material documenting the mineralisation in the Bierghes Sill has led to a re-evaluation of the mineral deposit model underpinning the analysis, in particular the role of lithological control and magmatic fluids, both previously thought to play important roles in the mineralisation process.

The mineralised veins and disseminated mineralisation are hosted by a wide variety of lithologies. Mineralisation in the Marcq area occurs as quartz veins within turbiditic sequences, whereas at Bierghes the mineralised quartz-carbonate veins occur within a dacite metaporphyry sill. Mineralised veins and associated disseminated mineralisation have also been recorded in tuffs, ignimbrites, sandstones, siltstones, slates, and quartzites. At a regional scale, a lack of

lithological control is apparent, although localised lithological associations may occur, possibly controlled by competence contrasts in the host rock succession.

In general, the association of magmatic rocks with mesothermal gold deposits is variable, although mineralization does often occur in close proximity. Within the Brabant Massif, magmatic rocks that are spatially associated with the known mineralisation occur along the southern margin, although they are thought to be at least 30 Ma older than the mineralisation. Piessens et al. (2002) draw analogies between the mineralising fluids at Sint-Pieters-Kapelle and those within the Phanerozoic polysulphide and gold mineralisation in the British Isles, which are often associated with granitic intrusions. Up until recently, the origin of the ore and fluids has been a matter of debate. Oxygen isotopic investigations by Piessens et al. (2000) revealed that the mineralising fluids fall primarily in the range typical for metamorphic fluids, although partial overlap occurred with that for primary magmatic fluids. More recent studies of sulphur isotopes by Dewaele et al. (2003) on eight mineral occurrences along the southern margin of the Anglo-Brabant Fold Belt (ABFB) revealed two sources of pyrite (sulphur): sedimentary pyrite with a bacteriogenic origin and an early diagenetic origin formed during hydrothermal circulation along high strain zones. Magmatic fluids can therefore be excluded as the dominant source or transport medium for the mineralisation (Dewaele and Muchez, 2004).

7.3.2 Key exploration parameters for mesothermal gold mineralisation

Taking into consideration the characteristics of mesothermal gold deposits and data availability, the following exploration parameters were selected as key indicators for use in prospectivity modelling:

Presence of shear zones/major structures (reflecting underlying anisotropy) from high resolution aeromagnetic and gravity lineaments and gravity horizontal gradient. No attempt was made to discriminate between high and low angle structures.

Occurrences of minerals associated with mesothermal style gold mineralisation and associated polysulphide mineralisation: gold, arsenopyrite, galena, sphalerite and chalcopyrite.

Gold analyses in drill core: values in excess of 10 ppb.

Record of pathfinder elements in hydrochemical samples for both mesothermal gold and associated polysulphide mineralisation: Au, As, Sb, Ag, Zn, Cu and Pb.

7.4 EVIDENTIAL DATA

7.4.1 Shear zones/major structures derived from geophysical lineaments

Outcrops in the vicinity of Sint-Pieters-Kapelle have revealed the presence of a NW-SE trending low-angle reverse shear zone, along which the polysulphide mineralisation occurs. The regional significance of this structure and its orientation have yet to be conclusively determined.

Two datasets were selected as indicators of potential shear zones/major structures: lineaments derived from reinterpreted high resolution airborne magnetic data as part of the 2003 project and gravity lineaments derived as part of this project.

The aeromagnetic lineaments comprising troughs, peaks, offsets and gradients were selected from the dataset (cultural and undefined lineaments were removed). The trough peaks and gradient lineaments were filtered to remove NW-SE lineaments within the Tubize Group, which were interpreted to represent lithological contacts; lineaments were removed in order to prevent undue bias towards the (unprospective) Tubize Group. All offset lineaments were used. The lineaments were buffered at 250 m intervals for a distance of 500 m. Each buffer was assigned fuzzy memberships reflecting the importance of faulting as evidence for defining the regional tectonic setting and as conduits for metal bearing hydrothermal fluids. Fuzzy memberships of

0.5 and 0.3 were assigned to the buffer zones around the structures, with membership values decreasing with increasing distance from the structure (Figure 9).

It was noted when calculating the 3-D slope depth solutions that, although the depths that were produced by the method are somewhat unreliable, the technique is good as an objective way of picking out lineations in the data. The manually-picked gravity lineaments, comprising maximum, minimum, local maximum, local minimum and inflections, were therefore filtered using slope depth solutions so that an individual lineament was accepted if there was a depth solution within a tolerance distance of 500 m. The resulting lineaments were then buffered at 500 m intervals for a distance of 1000 m. Fuzzy memberships of 0.3 and 0.2 were assigned to the buffer zones around the structures with membership values decreasing with increasing distance from the structure (Figure 10).

7.4.2 Age of host rocks

The pre-Permian subcrop map of the Brabant Massif that was published by De Vos et al. (1993) was selected as the geological base map (note that the resolution of this map does not discriminate between individual lithological units within the Ordovician and Silurian sequences, except for the Tremadocian, which consists exclusively of the Chevlipont formation (Lower Ordovician)). Linework from this map was captured (as vectors) using ArcGIS 8. Lithologies younger than the postulated age of mineralisation that potentially conceal the prospective Lower Ordovician sequences were assigned to the 'missing' data category. Areas assigned to the missing data category are given neither a negative or positive weighting.

7.4.3 Mineral Occurrences

Mineral occurrence data from boreholes made available for this study were filtered favouring vein style mineralisation. These vein occurrences, some of which have associated disseminated mineralisation, occur in rocks of Oisquercq, Ordovician and Silurian age and also within magmatic rocks. The main metalliferous minerals identified in these occurrences are sphalerite, galena, chalcopyrite and pyrite, and to a lesser extent pyrrhotite, marcasite, arsenopyrite and gold. Gold and arsenopyrite occurrences were selected as pathfinders for mesothermal gold, and chalcopyrite, galena and sphalerite were selected as pathfinders for the associated polysulphide mineralisation. The occurrences were buffered at 500 m for a distance of 1000 m. Sphalerite, galena and chalcopyrite, which tend to occur in association, were assigned fuzzy memberships of 0.2 and 0.1, which were combined using the fuzzy OR function (the highest value associated with these elements was thus selected for incorporation into the modelling process). Gold and arsenopyrite were assigned fuzzy memberships of 0.4 and 0.3, decreasing with increasing distance from the occurrence location; these values were not combined.

7.4.4 Gold in drill core

A veneer of Mesozoic and Tertiary sedimentary rocks masks the surface geochemical signature of the underlying geology, thus eliminating the use of surface geochemical analysis for use in the identification of zones of potential mineralisation. Gold analyses (ppb) from borehole core across the study area were provided, with up to seven analyses for each hole. The samples were obtained from a variety of lithologies, all from below the roof of the Lower Palaeozoic rocks (Table 7). The highest gold value (ppb) was selected from each borehole, independent of lithology. Of the 103 samples, 28 were above 10 ppb, the selected threshold below which samples were not included in the analysis. The three highest gold values, respectively 89 ppb, 250 ppb and 500 ppb, were from the Tremadoc in the Sint-Pieters-Kapelle area. The gold values were buffered at 500 m for a distance of 1000 m. Fuzzy memberships of 0.4 and 0.3 were assigned to the buffer zones around the borehole, with values decreasing with increasing distance from the borehole location.

	No. of boreholes
Cambrian	6
Interstratified volcanics	11
Magmatic samples	9
Oisquercq	19
Silurian	12
Tremadoc	6
Tubize	29
Upper Ordovician	6
Unclassified	5

Table 2 No of samples from each geological unit

7.4.5 Hydrochemistry

Hydrochemical analyses were provided for the study, from which the critical pathfinder elements for mesothermal gold were selected as Au, As, Sb. In addition, elements representing the associated polysulphide mineralisation were selected as Zn, Pb, Cu and Ag. Each element was gridded using the inverse distance weighting method of interpolation and was visually represented using quarter percent standard deviation intervals. A threshold was not applied, allowing the relationship of each element to the mineralisation, either positive or negative, to be incorporated into the analysis. Gold analyses from borehole core, graduated in size based on the concentration, were overlain with each hydrochemistry grid for visual examination (Figure 11, Figure 12, Figure 13 and Figure 14). The following observations were made for each of the selected elements:

- The anomalous gold values in the hydrochemical samples show little, if any, distinguishable positive correlation with the anomalous gold values in the borehole samples. This is to be expected, as there is little intrinsic indication of the source location in analyses of groundwater, due to possible transport of fluids away from their source. Gold in hydrochemical analyses was therefore not used;
- As, Sb and Pb display elevated concentrations in the northwest, north of Kortrijk;
- Pb and Zn display elevated concentrations in the extreme southeast around Tubize and Oisquercq;
- Ag and Cu display broadly similar patterns with anomalous concentrations in the central west and east; and
- Overall, the chalcophile elements, Zn, Pb, Cu and Ag show strong correlations with the area of known mineralisation. As and Sb show no positive correlation.

The base metals, Zn, Cu, Pb and Ag were combined using the Fuzzy OR function. Thus the highest value of these elements was selected for incorporation into the modelling process. As and Sb were also combined in the same manner. Incremental fuzzy memberships were assigned to the standard deviation intervals as in Table 3.

Standard Deviation	Fuzzy Membership

< Mean	0
Mean	0
0.00 – 0.25	0.1
0.25 – 0.50	0.1
0.50 – 0.75	0.1
0.75 – 1.00	0.2
1.00 – 1.25	0.2
1.25 – 1.50	0.2
1.50 – 1.75	0.3
1.75 – 2.00	0.3
2.00 – 2.25	0.3
2.25 – 2.50	0.4
2.50 – 2.75	0.4
2.75 – 3.00	0.4
> 3 St Dev	0.5

Table 3 Incremental fuzzy memberships used in combining elements

7.4.6 Gravity horizontal gradient

The magnitude of the horizontal gradient of gravity is an indicator of structure, as high gravity gradients are to be found where lithological units with different densities are brought into contact. Although this juxtaposition may be sedimentary, in which case the gradient is of limited interest, most often it is due to a tectonic or intrusional cause. Values greater than 0.546 were selected as a potential indicator of structure and were assigned a relatively low weighting of 0.2 reflecting the underlying uncertainty of the gradient (i.e. sedimentary or tectonic) but potentially important role in the mineralisation model.

7.5 FUZZY LOGIC MODEL RESULTS

The prospectivity model was produced using Fuzzy Logic operators. The hydrochemistry and mineral occurrence themes were combined as follows:

- Cu **OR** Pb **OR** Zn **OR** Ag
- As **OR** Sb
- Galena **OR** Sphalerite **OR** Chalcopyrite

The outputs from these Fuzzy OR operators were combined with the other fuzzy evidential themes using Fuzzy Algebraic Sum. The result of the prospectivity modelling is shown in Figure 15 for Fuzzy Algebraic Sum between 0 and 1. The prospectivity map for mesothermal gold and associated polysulphide mineralisation clearly indicates that structure is the predominant control, with areas of high prospectivity concentrated along gravity and magnetic lineaments. Areas with the greatest mineral potential (red) are concentrated in the southeast and northwest quadrants. In the southeast, the areas with the greatest potential occur around Geraardsbergen and Tubize, and south of Schepdaal, while in the northeast the areas with the greatest potential occur around and to the northeast of Kortrijk. Less prospective areas (grey) occur over the Tubize group in the northwest and over the Carboniferous sediments to the south of Ronse, where areas of further potential may occur at depth, beneath the younger cover.

The model output from this re-analysis was compared and contrasted with that produced the previous year (2003). The key differences in the datasets used in this analysis, with that carried out previously, can be summarised as follows: (i) the incorporation of re-interpreted high resolution gravity datasets, both the horizontal gradient and the derived gravity lineaments; (ii) the omission of the De Vos et al. (1993) fault dataset; and (iii) the omission of the Bouguer gravity anomaly dataset which was used as a potential indicator of low-density acidic intrusions which may have acted as a heat source to drive magmatic fluids.

A visual comparison of the outputs from both models was undertaken and the following observations were made (Figures 15 and 16):

- The prospective areas of both models are in strong agreement with the most prospective areas occurring in the southeast and northwest;
- The most prospective areas occur at structural intersections, in particular between different classes of magnetic lineaments and between gravity and magnetic lineaments. Further testing of the spatial relationship between first, second and third order structures and known mineralisation should be undertaken where possible ;
- Edge effects are less apparent on the revised prospectivity map, in particular the continuous linear features on the original output attributed to the De Vos et al. (1993) fault dataset;

The evaluation of the mineral potential of this region can only be determined by a detailed mineral exploration programme, in particular high resolution ground gravity and magnetic surveys to indicate or further refine the structural knowledge of the area. Mesothermal gold deposits may be a difficult deposit to evaluate due to the "nugget effect", hence the adage, “Drill for structure, drift for grade”.

8 Conclusions and further work

The principal conclusions of the work presented here are:

1 The results of 2½-D and 3-D modelling, and the analysis of Euler depth solutions, are consistent with interpretation of the overall gravity anomaly field over the southern Brabant Massif as due to a concealed granitic intrusion (of possible Caledonian age). The thickness of granite that is consistent with the observed anomalies is approximately 10 km.

2 Analysis of images of the data has underlined the importance of NW-SE major trending structures, which appear to offset the gravity low at the core of the Brabant Massif in a sinistral sense.

3 Removal of the regional field (here defined by upward-continuation of the observed data by 5 km) has revealed a wealth of short wavelength anomalies that were masked by the longer wavelengths present in the regional field (these mostly lie outside the full study area).

4 An analysis of mineral prospectivity has highlighted the relative importance of the NW and SE corners of the district as areas of enhanced mineral prospectivity. The Marcq structure is associated with a gravity residual high; analogous structures occur to the NNW along the Niewpoort-Asquempont lineament.

A number of further avenues of work should be pursued:

1 A seismic line should be acquired over the Brabant Massif, preferably passing directly over one of the gravity anomaly minima. Acquisition and processing parameters should be chosen so as to image the upper surface of the granite as predicted by interpretation of the potential field data. By doing this, it should be possible to get a strong sense of the nature of the subsurface and, if present, a good estimate of depth to the roof of the granite.

2 A deep borehole to investigate the nature of the basement rocks at depth is required. Until this is done, it is not possible to resolve arguments over the nature of the causative body. If the source is a buried granite then we would expect enhanced heat flow over the body, and hence it may have geothermal applications. The relatively stable environment provided by

a granite over geological time periods may also provide conditions for long-term waste disposal.

3 Analysis of mineral prospectivity could be improved by acquisition of detailed gravity and ground magnetic surveys that would greatly improve knowledge of local structure. For example, the local gravity high lying to the NW of Marq should be investigated using detailed ground geophysics.

4 There is scope for a systematic campaign of geochemical investigations in the Brabant Massif. This would allow identification and mapping of geochemical anomalies due to mineralization, as well as highlighting those areas where there are possible hazards due to human activity.

Appendix 1 ArcView project GIS

This Appendix lists the various layers (themes) that are present in the project GIS that accompanies this report and is supplied on CD. The GIS is entirely contained within the directory SBM_GIS; this directory contains an ArcView project file (`sbmg.apr`) that references data sets contained in the subdirectories of that directory. Feature information is stored in the directory FEATURES and images in directory IMAGES. No BGS-developed extensions are required in order to operate correctly, but the user may need to load the extensions that allow handling of TIFF and JPEG images within ArcView.

This GIS was developed using ArcView version 3.3 running under Windows 2000.

LIST OF FEATURES

These themes are in the subdirectory FEATURES

File	Description	Comments
3dmodel_area.shp	Modelling area for 3-D modelling study.	
anre_pnts_ed.shp	Scattered gravity data points.	Final edited set.
anre_pnts_ed_lim.shp	Limits of scattered data set.	
area.shp	Study area.	58 – 146 kmE, 148 – 185 kmN
cities.shp	Locations of cities.	
coast_mask.shp	Mask at coastline to hide offshore data.	
ge3d_si10.shp	3-D gravity Euler solutions.	Structural index 1.
glinears.avl	Legend file for classification of linears.	
gmt_borders.shp	Borders from the GMT public-domain package.	
gmt_coastline.shp	Coastline from the GMT public-domain package.	
grav_highs_1.shp	Gravity highs.	Plot first
grav_highs_2.shp	Gravity highs.	Plot second
grav_lows_1.shp	Gravity lows.	Plot first
grav_lows_2.shp	Gravity lows.	Plot second
grav_lows_3.shp	Gravity lows.	Plot third
grav_outline.shp	Outline of scattered data.	
gravlins_v1.shp	Gravity linears.	
mapsheets.shp	Map sheet boundaries.	
profiles.shp	Location of model profiles.	Includes all published profiles.
provinces.shp	Provincial borders	

LIST OF IMAGES

These themes are in the directory IMAGES

File	Description	Comments
belg_grav_as.jpg	Analytic signal.	
belg_grav_hg.jpg	Horizontal gradient.	
belg_grav_obs.jpg	Observed gravity.	Reduction density 2100 kg m^{-3}.
belg_grav_res1k.jpg	Residual gravity after subtraction of anomalies upward continued by 1 km.	
belg_grav_res5k.jpg	Residual gravity after subtraction of anomalies upward continued by 5 km.	
belg_grav_res5k_eqint3.jpg	Residual gravity after subtraction of anomalies upward continued by 5 km.	Displayed with an equal interval colour scale.
belg_grav_u100_1d.jpg	1^{st} vertical derivative.	
belg_grav_u500_2d.jpg	2^{nd} vertical derivative.	

Note that for each image there is a separate image of the appropriate colour scale stored in the same directory. These are recognisable as TIFF files with names ending in "_scale.tif".

References

ANDRÉ, L and DEUTSCH, S. 1985. Very low-grade metamorphic Sr isotopic resettings of magmatic rocks and minerals: evidence for a late Givetian strike-slip division of the Brabant Massif, Belgium. *Journal of the Geological Society, London* 142, 911-924.

BLAKELY, R J. 1995. Potential theory in Gravity and Magnetic Applications. Cambridge University Press, UK. ISBN 0-521-57547-8.

CHACKSFIELD, B C, DE VOS, W, D'HOOGE, L, DUSAR, M, LEE, M K, POITEVIN, C, ROYLES, C P, and VERNIERS, J. 1993. A new look at Belgian aeromagnetic and gravity data through image-based display and integrated modelling techniques. *Geol. Mag*. Vol 130, 583-591.

COX, D P and SINGER, D A (eds). 1986. Mineral deposit models. *USGS Bulletin* Vol 1693, 379

D'ERCOLE, C, GROVES, D I, KNOX-ROBINSON, C M. 2000. Using fuzzy logic within a GIS-environment to enhance conceptually based prospectivity analysis of MVT mineralisation. *Australian Journal of Earth Sciences,* Vol 47, 913-927

DEBACKER, T N. 1999. Folds trending at various angles to the transport direction in the Marcq area, Brabant Massif, Belgium. *Geologica Belgica* 2, 159-172.

DEBACKER, T N, HERBOSCH, A, SINTUBIN, M and VERNIERS, J. 2003. Palaeozoic deformation in the Asquempont-Virginal area (Brabant Massif, Belgium). A Field Guide. F.N.R.S. Caledonides Group. Belgian Structural Geology Study Group, *Geologica Belgica.* 29pp.

DE VOS, W, VERNIERS, J, HERBOSCH, A, and VANGUESTAINE, M. 1993. A new geological map of the Brabant Massif, Belgium. *Geol. Mag*. Vol 130, 605-611.

DE VOS, W, CHACKSFIELD, B C, D'HOOGE, L, DUSAR, M, LEE, M K, POITEVIN, C, ROYLES, C P, VANDENBORGH, T, VAN EYCK, J, and VERNIERS, J. 1993. Image-based display of Belgian digital aeromagnetic and gravity data. *Belgische Geologische Dienst Professional Paper*, 1993/5 – N.263.

DE VOS, W, POOT, B HUS, J, A, and KHAYATI, M. EL 1992. Geophysical characterisation of lithologies from the Brabant Massif as a contribution to gravimetric and magnetic modelling. *Bulletin de la Société belge de Géologie*, T. 101(3-4), 173-180.

DANDOIS, P. 1997. Etude de minéralisations dans le Massif de Brabant. *Unpublished report of the Geol. Survey of Belgium*, project NAT/94-2.1. Univ. Liège (includes “dossiers techniques” on 26 drillholes studied with polished sections).

DEWAELE, S, MUCHEZ, P AND BOYCE, A. 2003. Interplay between sulphur sources in polysulphide mineralisation in the Lower Palaeozoic of the Anglo-Brabant Fold belt, Belgium. *Journal of Geochemical Exploration.* Vol 78-79, 607-611

DEWAELE S AND MUCHEZ P. 2004. Alteration, mineralisation and fluid flow characteristics in the Bierghes Sill, Anglo-Brabant Fold belt, Belgium. *Geologica Belgica*. Vol 7/1-2, 55-69

EVERAERTS, M, POITEVIN, C, DE VOS, W and STERPIN, M. 1996. Integrated geophysical/geological modelling of the western Brabant Massif and structural implications. *Bulletin de la Société belge de Géologie*, T. 105(1-2), 41-59.

GROVES, D I, GOLDFARB, R J, KNOX-ROBINSON, C M, OJALA, J, GARDOLL, S, YUN, G Y, AND HOLYLAND, P. 2000. Late kinematic timing of orogenic gold deposits and significance for computer-based exploration techniques with emphasis on the Yilgarn Block, Western Australia. *Ore Geology Reviews,* , Vol 17(1-2), 1-38.

GROVES, D I, GOLDFARB, R J, GEBRE-MARIAM, M, HAGEMANN, S G AND ROBERT, F. 1998. Orogenic gold deposits: A proposed classification in the context of their crustal distribution and relationship to other gold deposit types. *Ore Geology Reviews*, 13, 7-27

GUNN, A. G, AND ROLLIN, K.E. 2000. Exploration methods and new targets for epithermal gold mineralisation in the Devonian rocks of northern Britain. *Minerals Programme Publication No 2 British Geological Survey RR/00/08*.

HODGSON, C J. 1993. Mesothermal lode gold deposits. *Mineral Deposits Modelling*, Special Paper 40. Geological Association of Canada, 635-678.

KEMP, L D, BONHAM-CARTER, G F, RAINES, G L AND LOONEY, C G. 2001. Arc-SDM: Arcview extension for spatial data modelling using weights of evidence, logistic regression, fuzzy logic and neural network analysis. http://ntserv.gis.nrcan.gc.ca/sdm/

KEPPIE, J D, BOYLE, R W and HAYNES, S J. 1986. Turbidite-hosted gold deposits. *Geological Association of Canada Special Paper,* No. 32.

LEE, M K, PHARAOH, T C, WILLIAMSON, J P, GREEN, C A, and DE VOS, W. 1993. Evidence on the deep structure of the Anglo-Brabant Massif from gravity and magnetic data. *Geol. Mag*. Vol 130, 575-582.

LEGRAND, R. 1968. Le massif du Brabant. *Mémoire, Service Géologique de Belgique* no. 9.

MCMILLAN, R H. 1996. Turbidite-hosted Au veins. In: LEFEBURE, D V and HOY, T. (editors) Selected British Columbia mineral deposit profiles, volume 2 – metallic deposits. *British Columbia Energy and Mines Division Open File*, No. 1996-13, 59–62.

MANSY, J L, EVERAERTS, M, and DE VOS, W. 1999. Structural analysis of the adjacent Acadian and Variscan fold belts in Belgium and northern France from geophysical and geological evidence. *Tectonophysics* Vol 109, 99-116.

NESBITT, B E. 1991. Phanerozoic gold deposits in tectonically active contintenal margins. In: FOSTER, R P. *Gold metallogeny and exploration*, Blackie, Glasgow and London, 104–132.

PHARAOH, T C, MOLYNEUX, S G, MERRIMAN, R J, LEE, M K and VERNIERS, J. 1993. The Caledonides of the Anglo-Brabant Massif reviewed. *Geol. Mag*. Vol 130, 561-562.

PHARAOH, T C, ENGLAND, R and LEE, M K. 1995. The concealed Caledonide basement of eastern England and the southern North Sea - a review. *In:* Gee, D.G. & Beckholmen, M. (eds). The Trans-European Suture Zone. Europrobe in Liblice 1993. *Studia Geophysica et Geodaetica*, 39, 330-346.

PHARAOH, T C. 1999. Palaeozoic terranes and their lithospheric boundaries within the Trans-European Suture Zone (TESZ): a review. *Tectonophysics* 314, 7-29.

PIESSENS, K, MUCHEZ, P, VIAENE , W, and DE VOS, W. 1999 . Syntectonic polysulphide mineralisation in the Brabant Massif, Belgium Mineral Deposits: Processes to Processing, Stanley et al. (eds), 963-966

PIESSENS, K, MUCHEZ, P, VIAENE, W. BOYCE, A, DE VOS, W , SINTUBIN, M and DEBACKER, T. 2000. Alteration and fluid characteristics of a mineralised shear zone in Lower Palaeozoic of the Anglo-Brabant belt, Belgium *Journal of Geochemical Exploration* Vol 69, 317-321.

PIESSENS, K, MUCHEZ, P, DEWAELE, S, BOYCE, A, DE VOS, W, SINTUBIN, M, DEBACKER, TN, BURKE, EAJ, and VIAENE, W. 2002. Fluid flow, alteration and polysulphide mineralisation associated with a low-angle reverse shear zone in the Lower Palaeozoic of the Anglo-Brabant fold belt, Belgium. *Tectonophysics* Vol 348, 73-92.

ROBERT, F, POULSEN, K H, AND DUBE, B. 1997. Gold deposits and their geological classification. Proceedings of Exploration 97: Fourth Internation Conference on mineral Exploration. 209-220

ROLLIN, K E. 1988. GM3D: Forward and iterative 3-D gravity and magnetic modelling using vertical square prisms. *British Geological Survey Technical Report* WK/88/17

ROLLIN, KE. GUNN, A.G, SCRIVENER, RC, AND SHAW, MH. 2001. Potential for stratiform massive sulphide mineralisation in south-west England. *Minerals Programme Publication No 9 British Geological Survey CR/01/240.*

SINTUBIN, M. 1999. Arcuate fold and cleavage patters in the southeastern part of the Anglo-Brabant Fold Belt (Belgium): tectonic implications. *Tectonophysics* Vol 109, 81-97.

TANGESTANI, M H AND MOORE, F. Mapping porphyry copper potential with a fuzzy model, northern Shahr-e-Babak, Iran. *Australian Journal of Earth Sciences,* 2003, 50(3), 311-317.

VERCOUTERE, C, and VAN DEN HAUTE, P. 1993. Post-Palaeozoic cooling and uplift of the Brabant Massif as revealed by apatite fission track analysis. *Geol. Mag*. Vol 130, 639-646.

VERNIERS, J, HERBOSCH, A, VANGUESTAINE, M, GEUKENS, F, DELCAMBRE, B, PINGOT, J-L, BELANGER, I, HENNEBERT, M, DEBACKER, T, SINTUBIN, M and DE VOS, W. 2001. Cambrian-Ordovician-Silurian lithostratigraphic units (Belgium). *Geologica Belgica* Vol 4, 5-38. ISSN 1374-8505

WESSEL, P, and SMITH, W H F. 1991. Free software helps map and display data. *EOS Trans. AGU*, Vol 72, 441.

WILLIAMSON, J P, CHACKSFIELD, B C, MCEVOY, F M and PHARAOH, T C. 2003. Reinterpretation of airborne magnetic data over the Brabant Massif in southern Flanders (Belgium). *British Geological Survey Commissioned Report* CR/03/135.

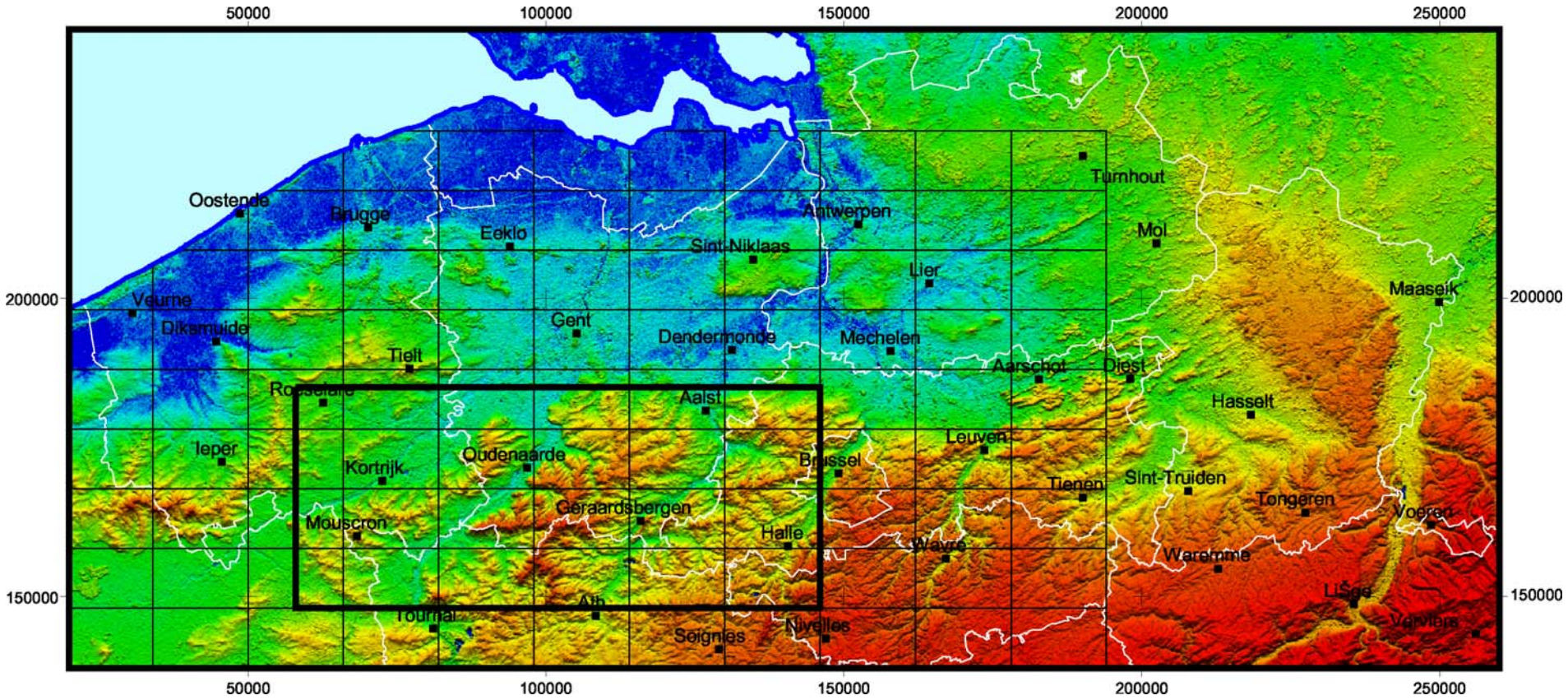

Figure 1: Location of the study area. The bold black line outlines the area that was covered by the detailed study; thin black lines mark the extent of individual geological map sheets. The topographic image forming the background is of a 100 m DEM that was computed using data from the Shuttle Radar Topography Mission (native resolution approximately 90 m).

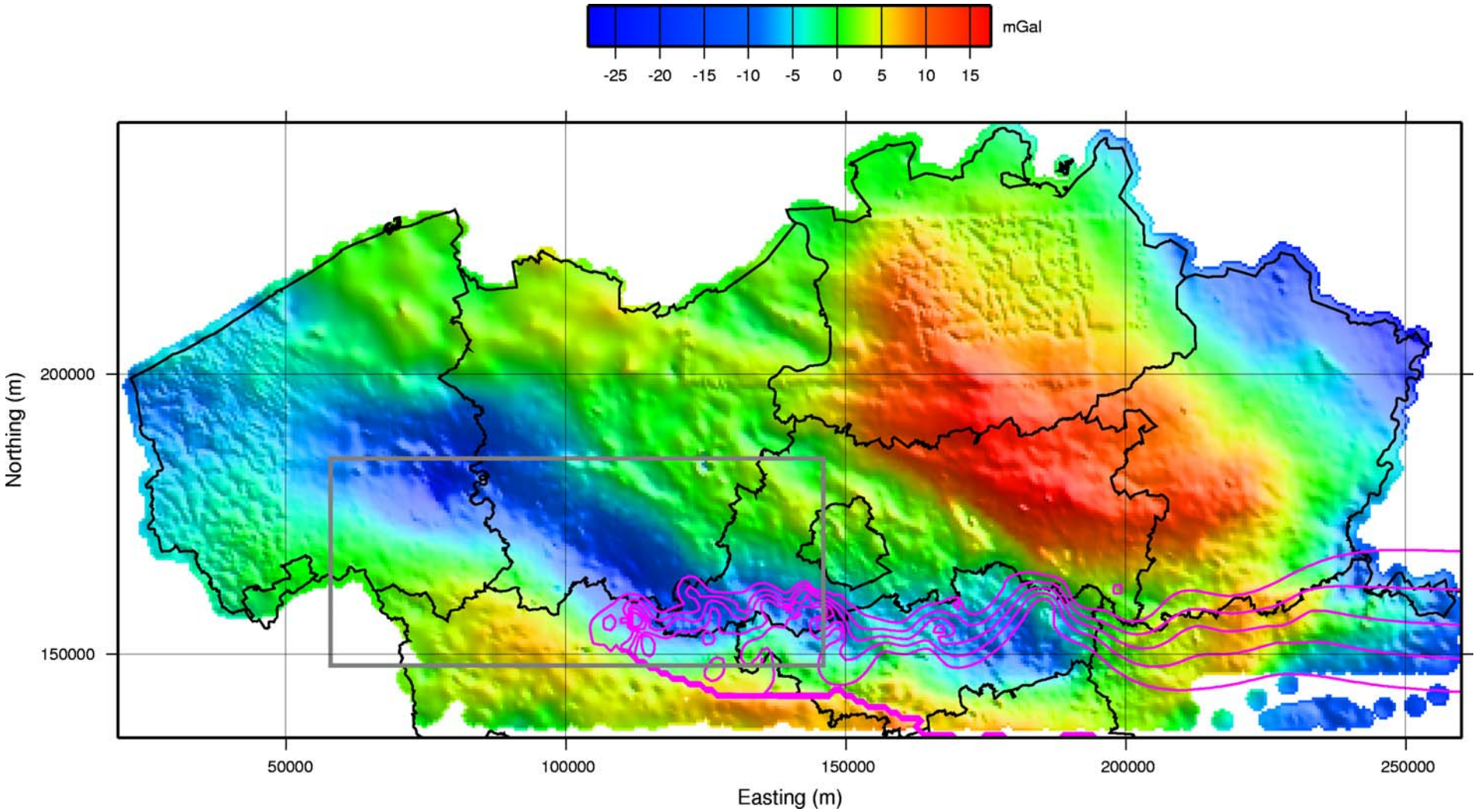

Figure 2: Results of applying a variable density Bouguer reduction to the scattered data. Contours are of reduction density, varying from 2670 kg,m^{-3} in the SE to 2100 kg.m^{-3} (100 kg.m^{-3} interval). Outside the Brabant Massif and south of 150000 mN a density of 2670 kg.m^{-3} was used. See text for discussion.

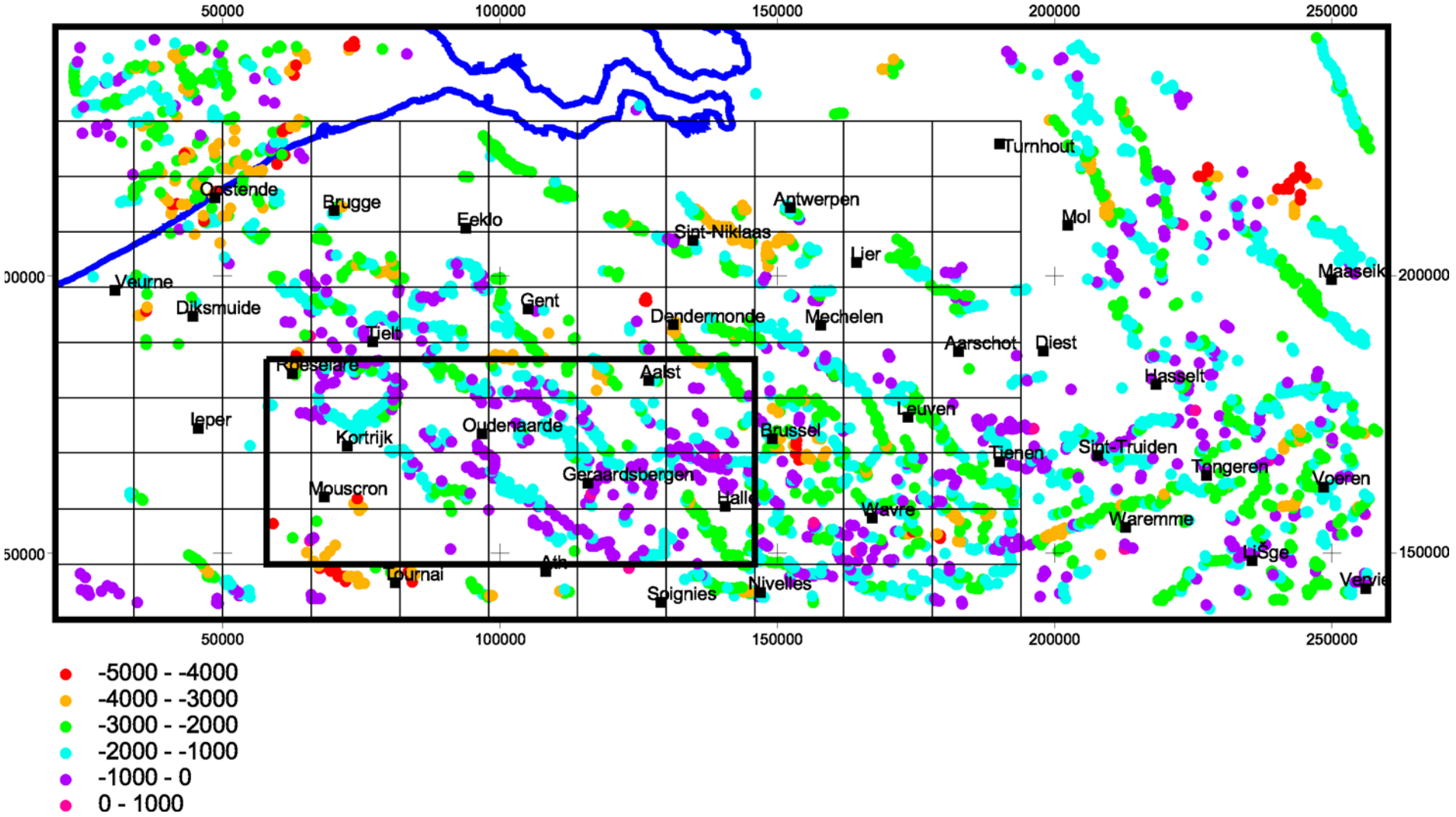

Figure 3: 3-D Euler solutions calculated using a structural index of 1. Indicated depths are in metres. The negative anomaly ESE of Roeslare and N of Kortrijk is seen to be delineated by a ring of solutions with depths mostly < 2000 m. Depths associated with the negative anomaly that cores the Brabant Massif generally increase moving eastwards.

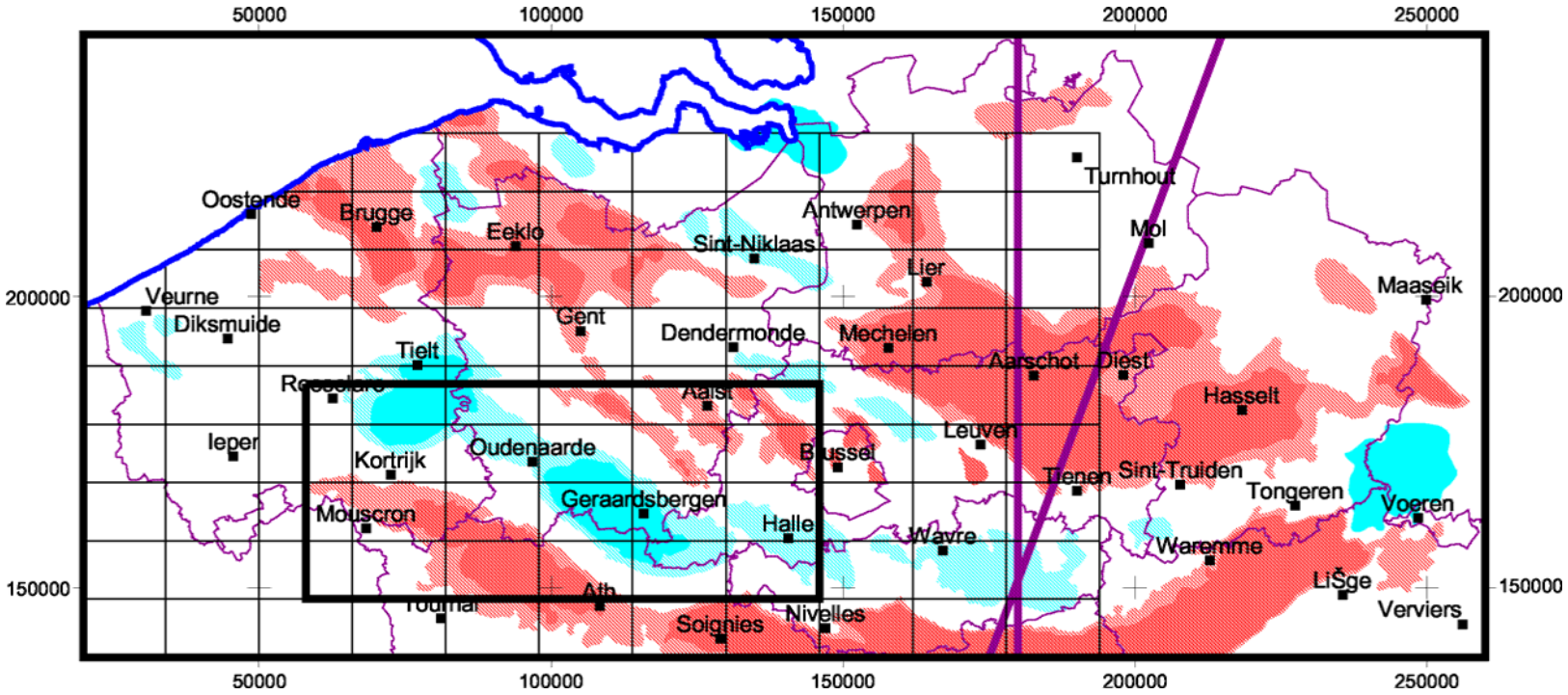

Figure 4: 2½-D model profiles are displayed as thick purple lines overlain on a schematic representation of the major gravity anomalies (positive red, negative blue). Profile 1 is from [180000 138000] to [180000 245000] and profile 2 is from [175000 138000] to [215000 245000].

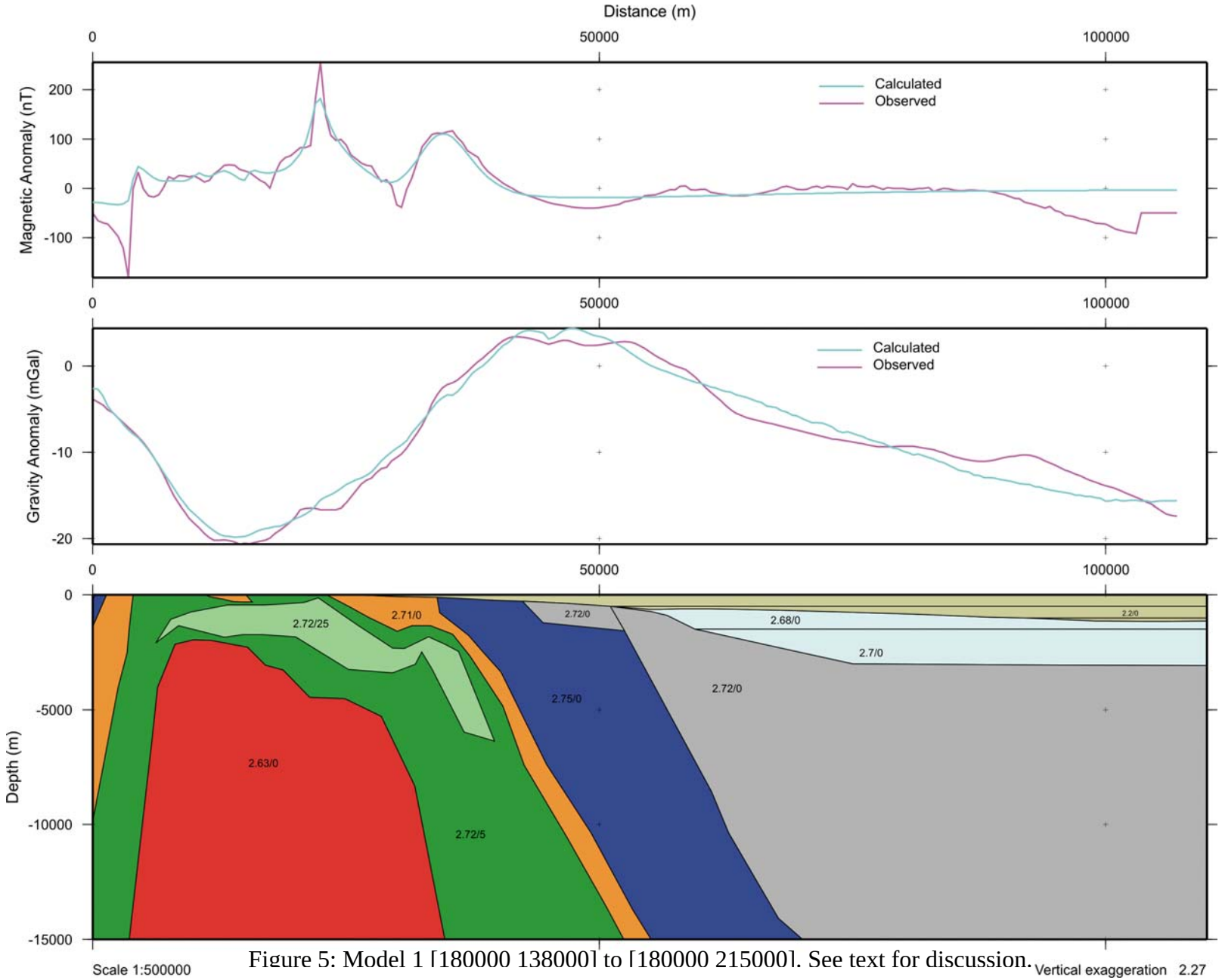

Figure 5: Model 1 ⌈180000 138000⌉ to ⌈180000 215000⌉. See text for discussion.

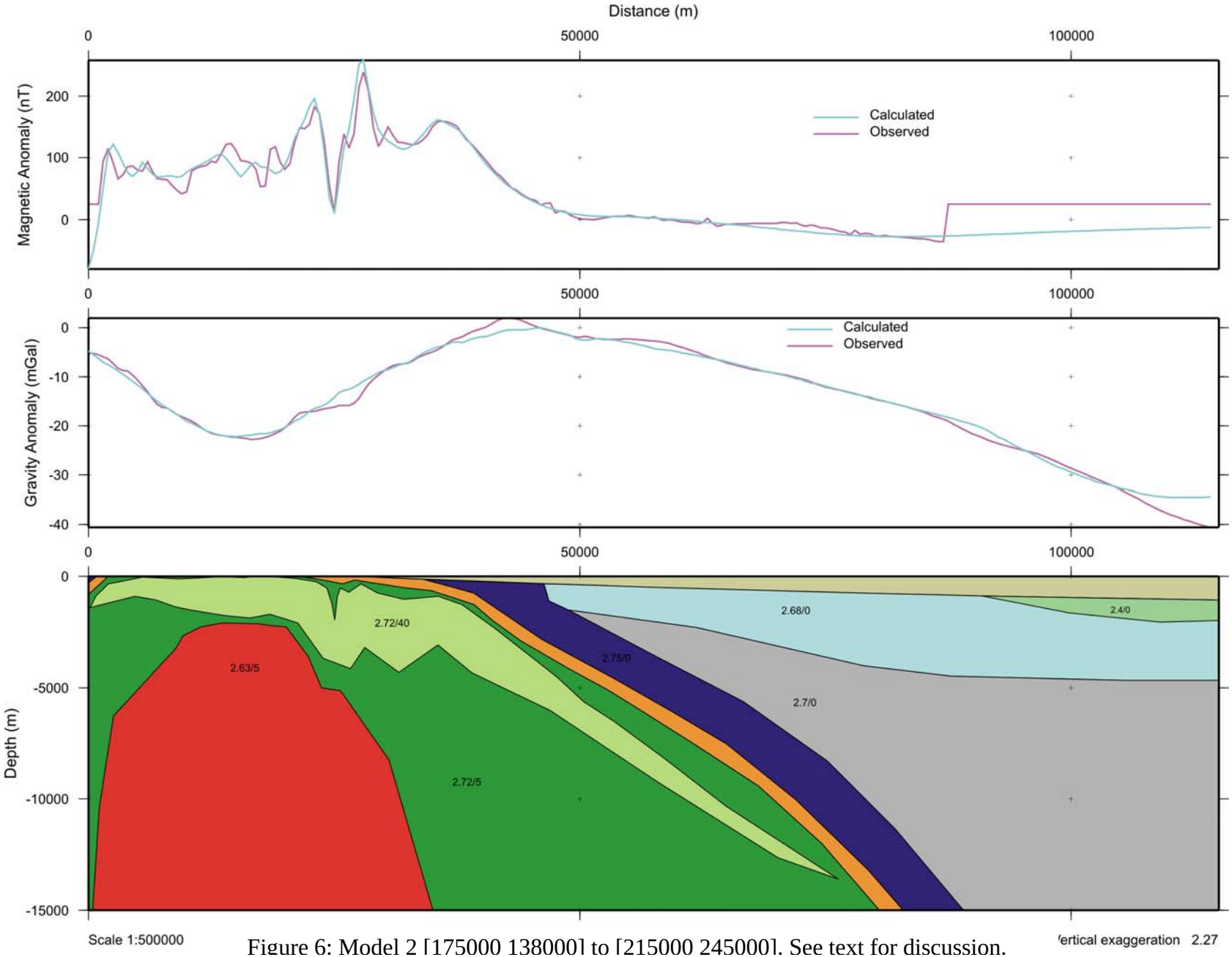

Figure 6: Model 2 [175000 138000] to [215000 245000]. See text for discussion.

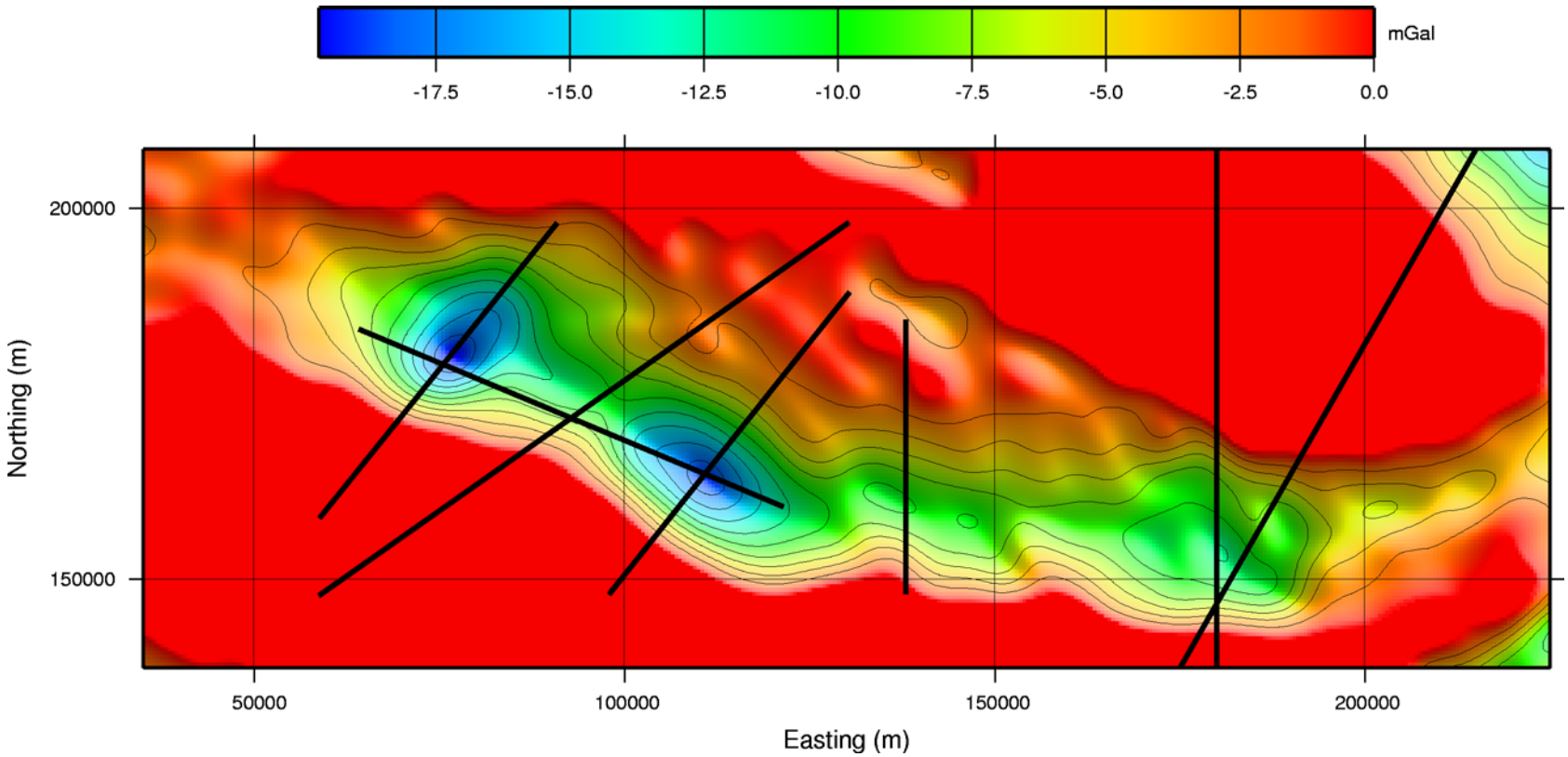

Figure 7: Residual anomaly used as input to 3-D modelling.

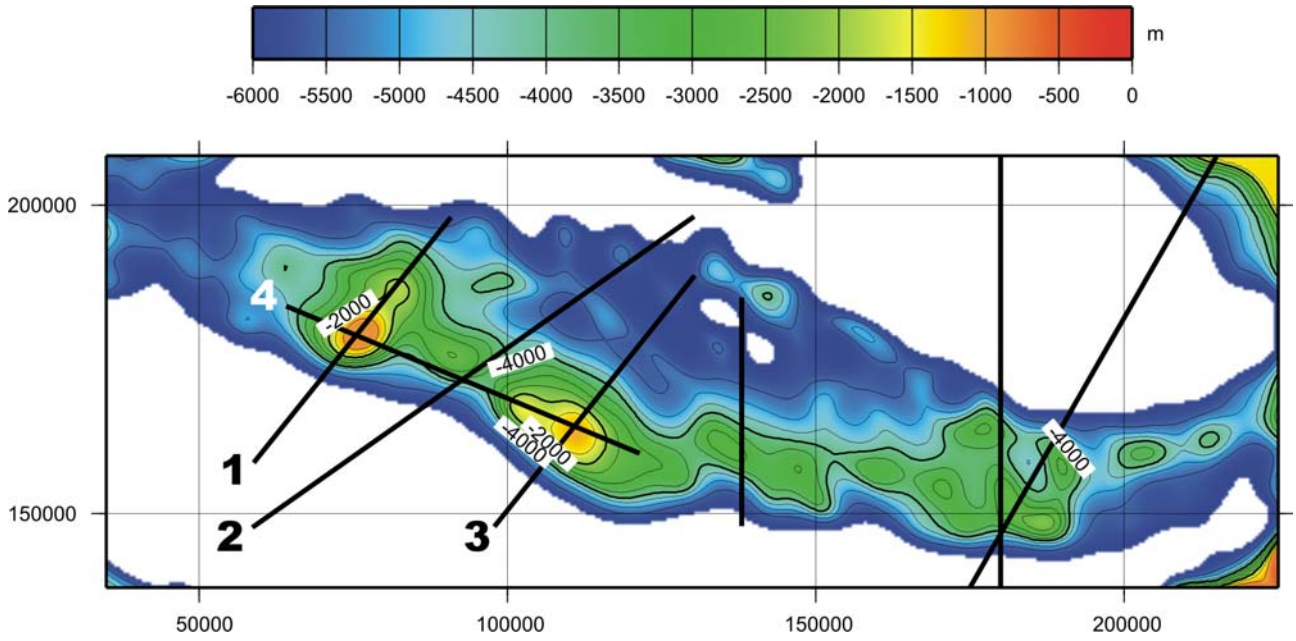

Figure 8a: Depth to the top of the modelled low-density layer.

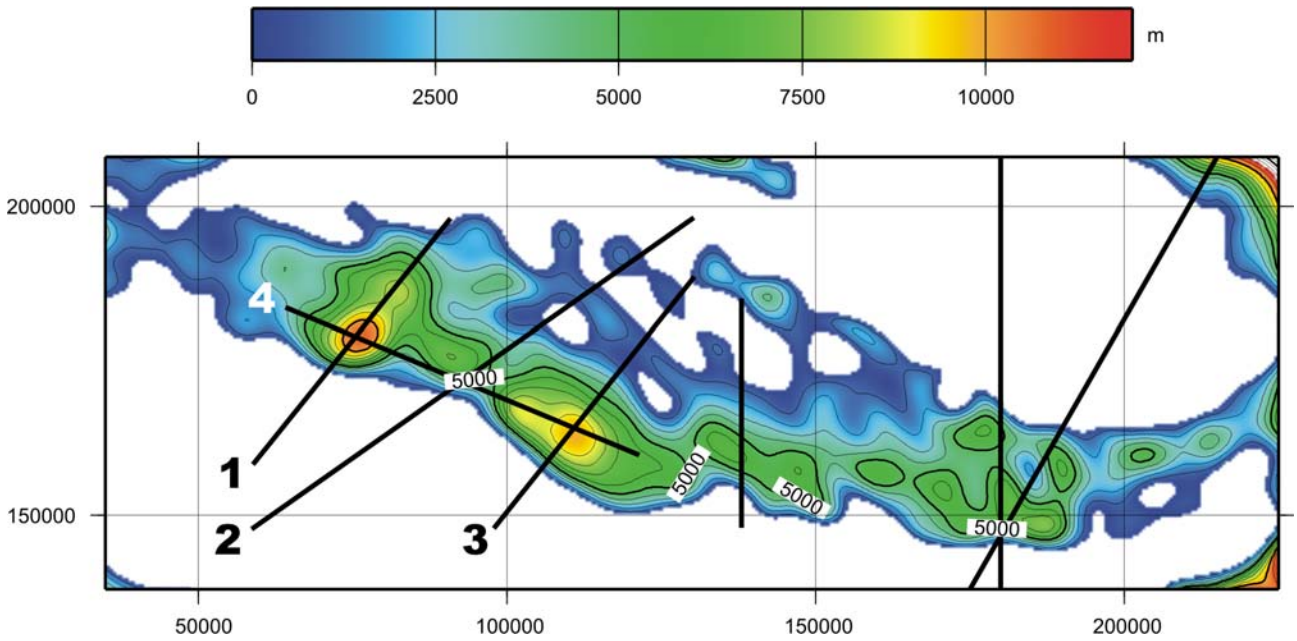

Figure 8b: Thickness of the modelled low-density layer.

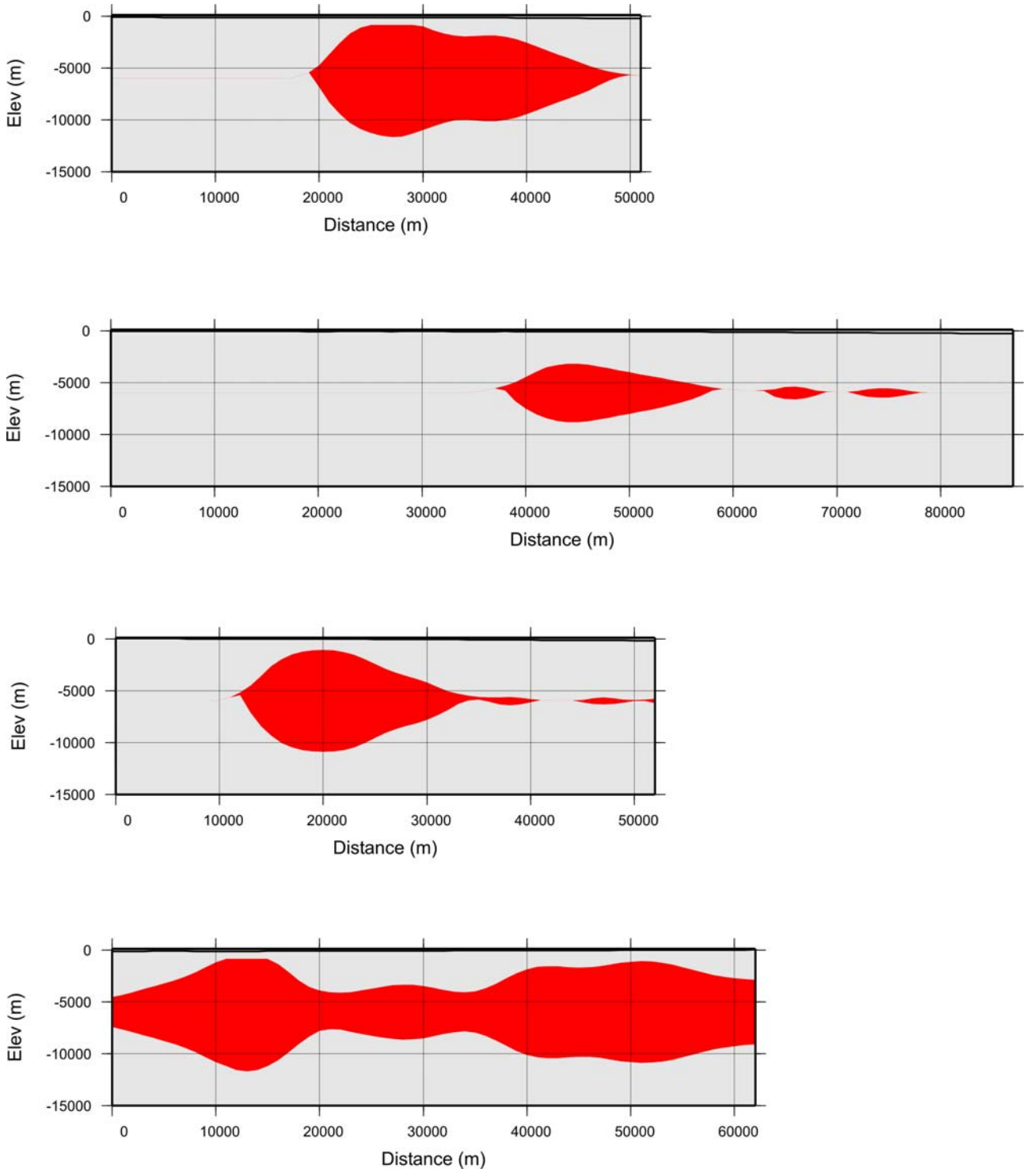

Figure 9: Sections through the 3-D model along profiles 1 (top) to 4 (bottom), lines which are coincident with those published by Everaerts et al. (1996).

a

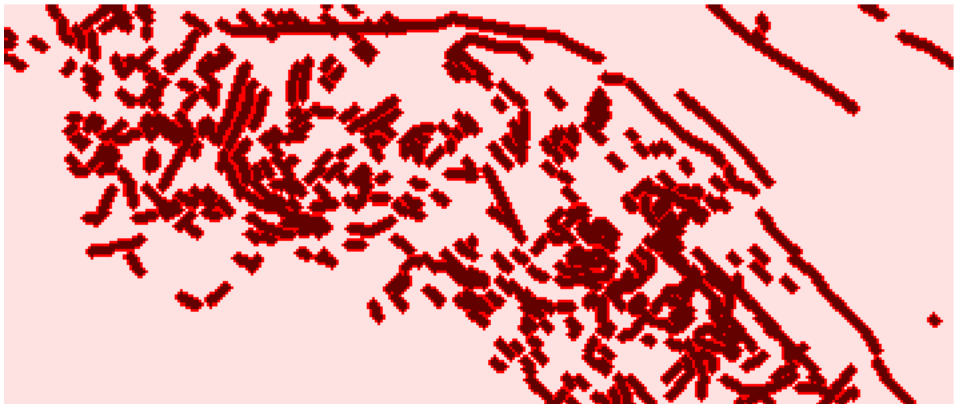

b

c

d

Figure 10: Fuzzy memberships applied to buffered (a) gradient; (b) offset; (c) peak and (d) trough magnetic linears.

Figure 11: Fuzzy memberships applied to buffered gravity linears.

a

b

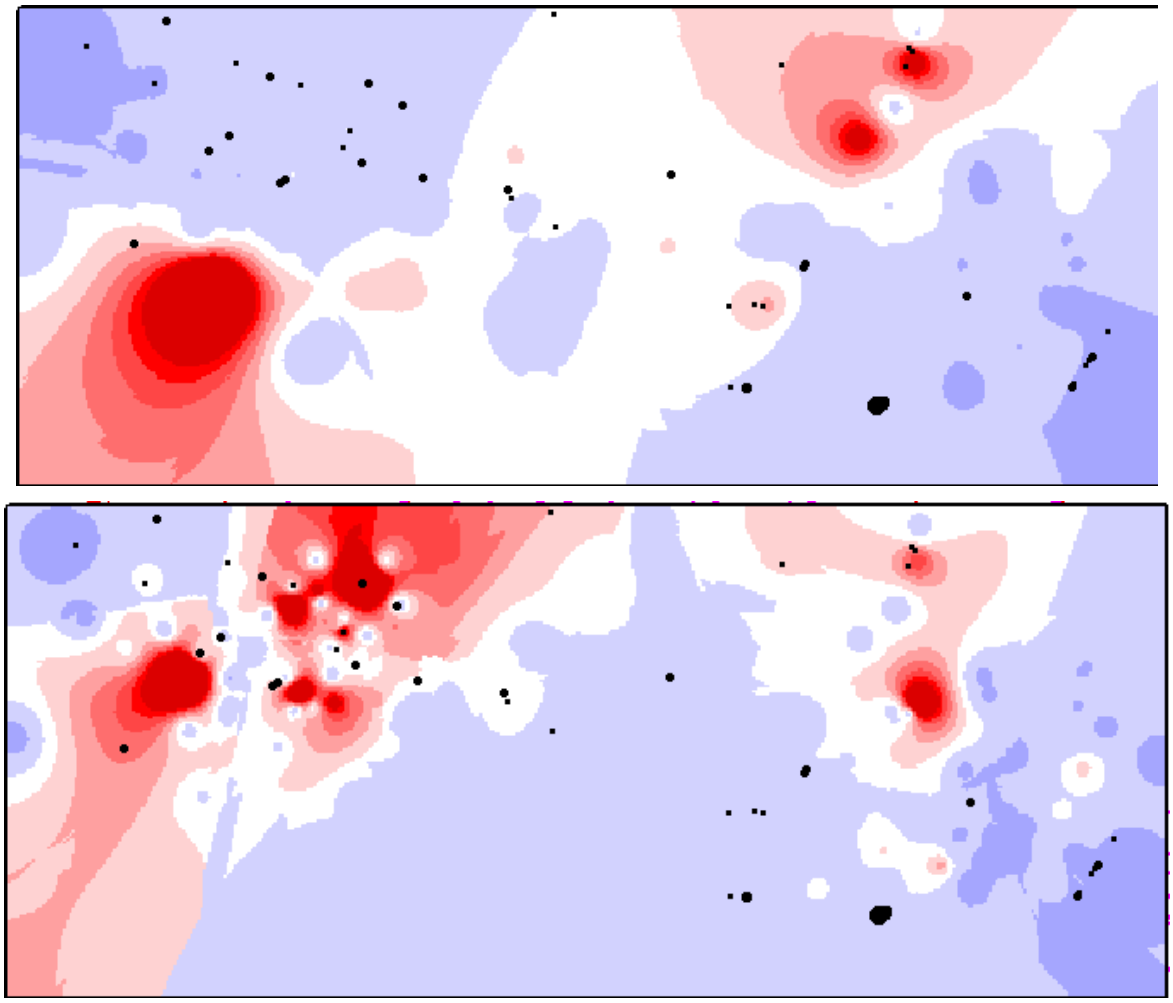

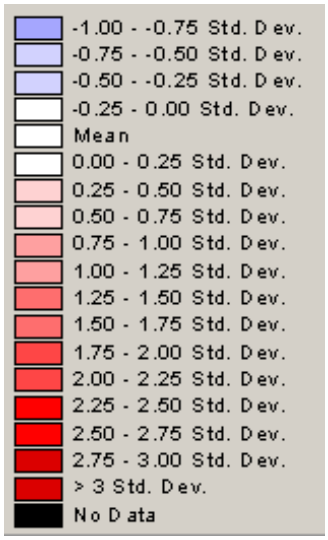

Figure 12: Plots showing the distribution of hydrochemical analyses, displayed using quarter standard deviation values for Au (a) and Sb (b).

a

b

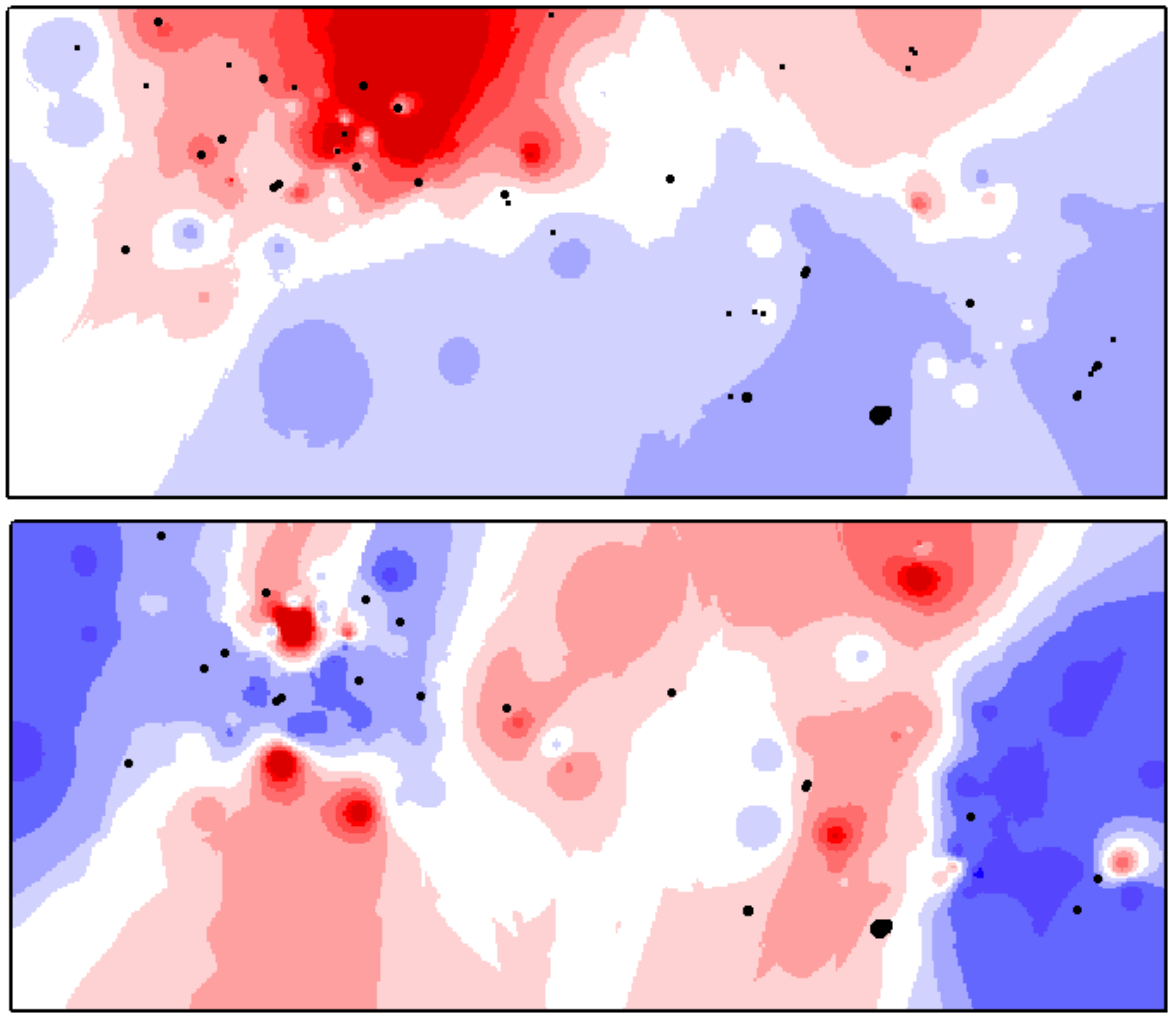

Figure 13: Plots showing the distribution of hydrochemical analyses, displayed using quarter standard deviation values for As (a) and Ag (b).

a

b

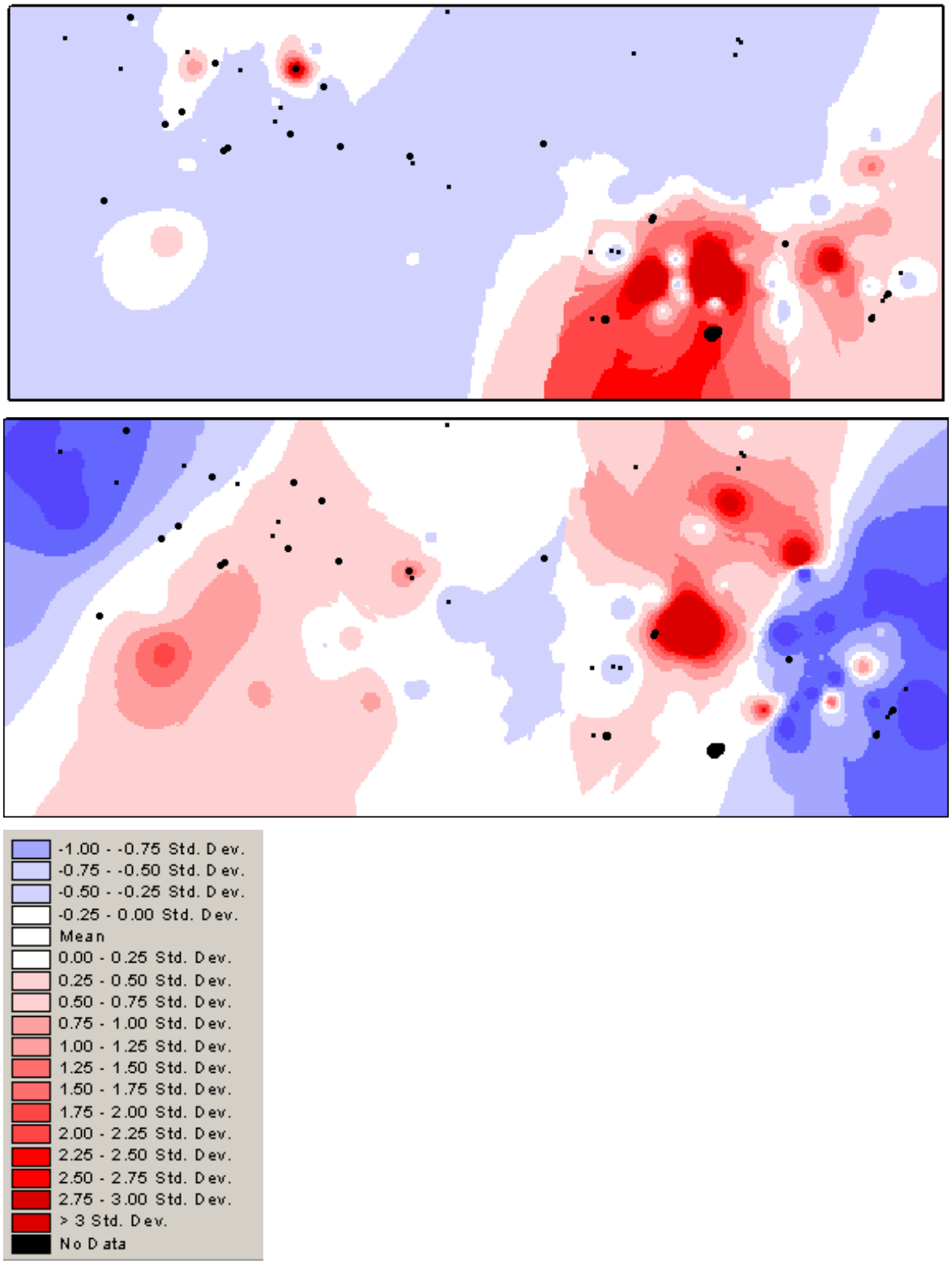

Figure 14: Plots showing the distribution of hydrochemical analyses, displayed using quarter standard deviation values for Zn (a) and Cu (b).

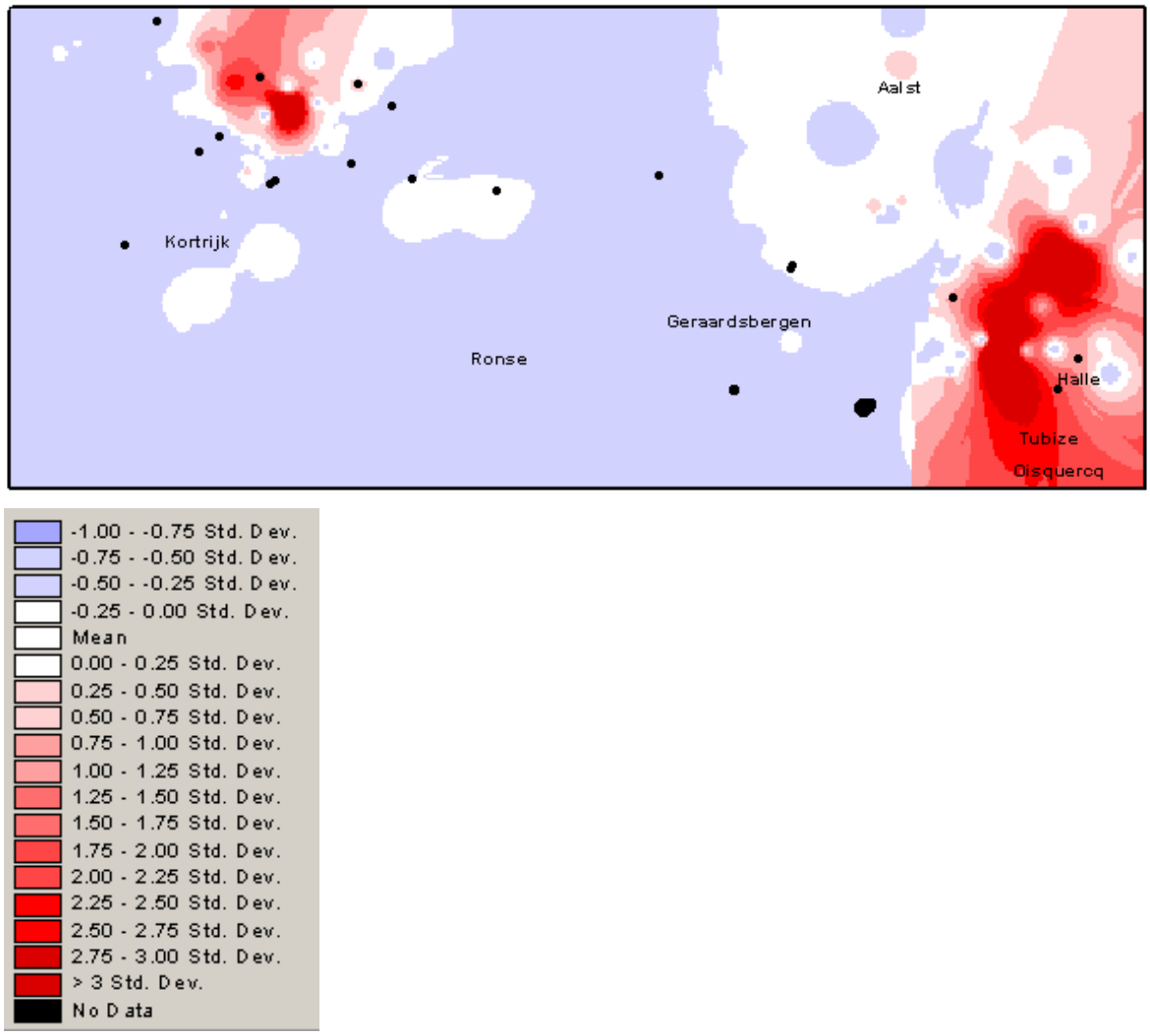

Figure 15: Plot showing the distribution of hydrochemical analyses, displayed using quarter standard deviation values for Pb.

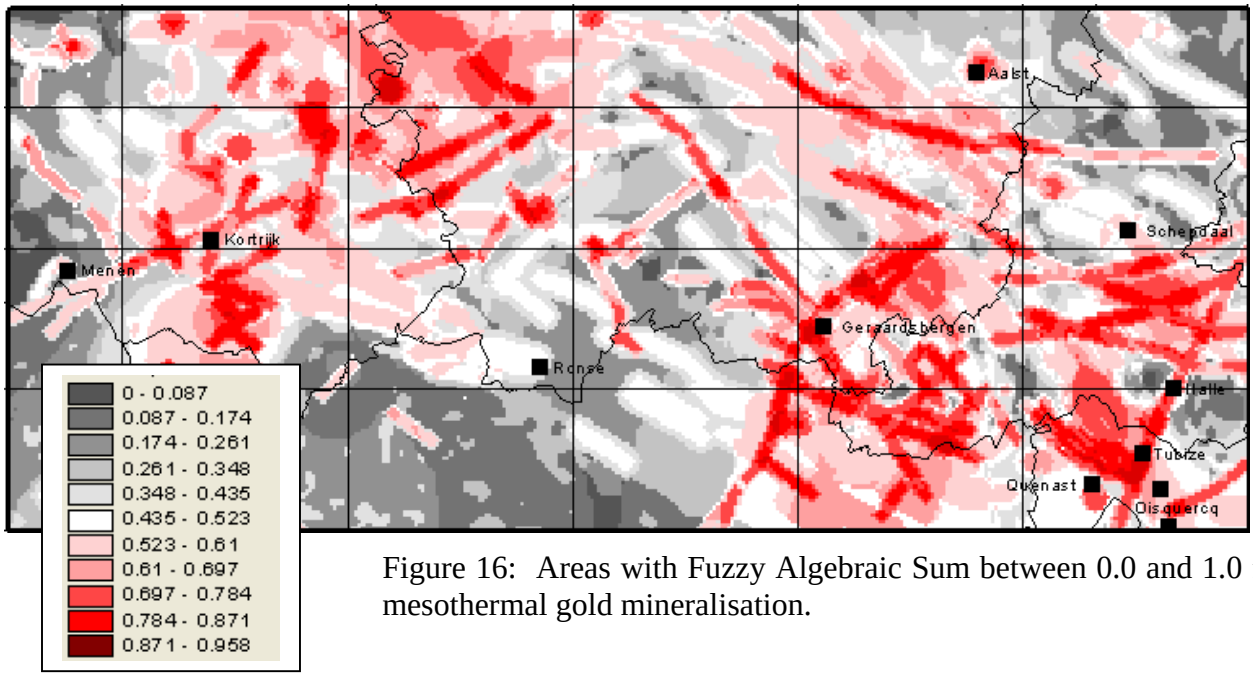

Figure 16: Areas with Fuzzy Algebraic Sum between 0.0 and 1.0 for mesothermal gold mineralisation.

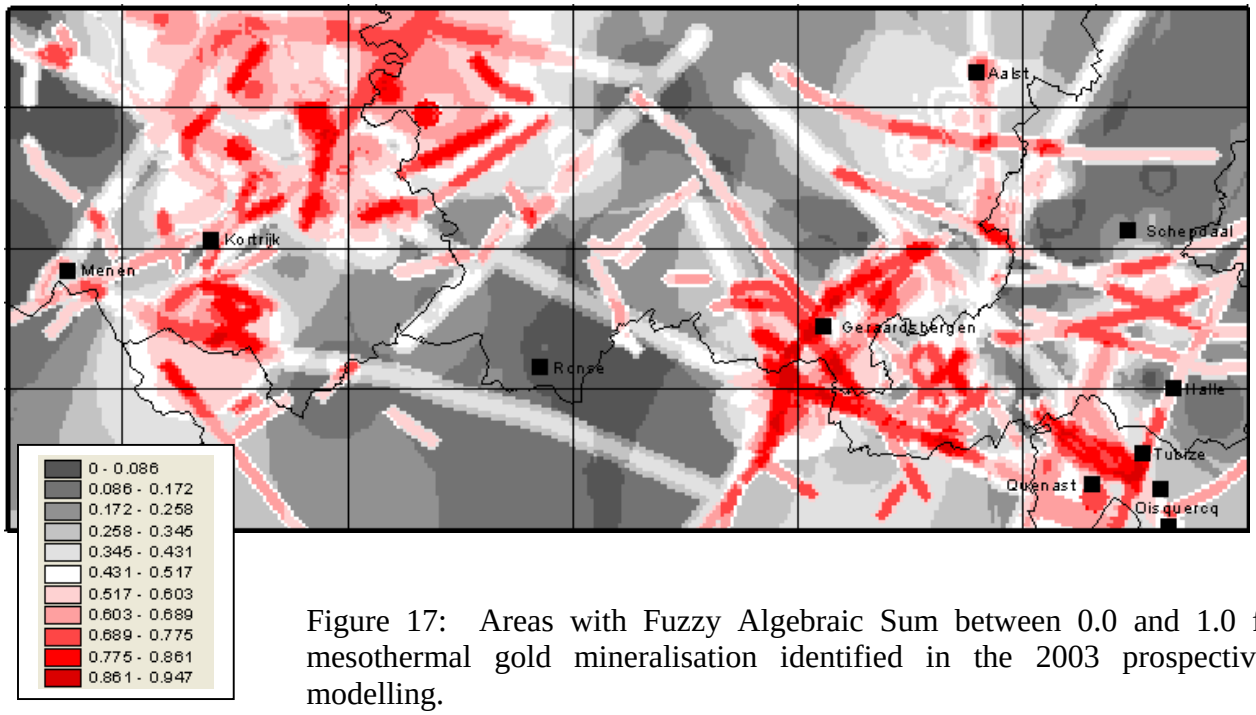

Figure 17: Areas with Fuzzy Algebraic Sum between 0.0 and 1.0 for mesothermal gold mineralisation identified in the 2003 prospectivity modelling.